Modelling the impact of topography on seismic amplification at regional scale

Dita Anggraeni
February, 2010

Modelling the impact of topography on seismic amplification at regional scale

by

Dita Anggraeni

Thesis submitted to the International Institute for Geo-information Science and Earth Observation in partial fulfilment of the requirements for the degree of Master of Science in Geo-information Science and Earth Observation, Specialisation: Geo-hazards

Thesis Assessment Board

Prof.Dr. F.D. van der Meer (Chair)
S. Kroonenberg (External Examiner)

Dr. M. van der Meijde (Supervisor)
MSc W.H. Bakker (Second supervisor)

Drs. T.M. Loran (Observer)

INTERNATIONAL INSTITUTE FOR GEO-INFORMATION SCIENCE AND EARTH OBSERVATION
ENSCHEDE, THE NETHERLANDS

Disclaimer

This document describes work undertaken as part of a programme of study at the International Institute for Geo-information Science and Earth Observation. All views and opinions expressed therein remain the sole responsibility of the author, and do not necessarily represent those of the institute.

Abstract

Earthquake triggered ground shaking depends not only on the characteristics of earthquake source parameters and medium of seismic waves propagation, but also on the site effects. These site effects are often not included in regional ground shaking models, especially local topography, where hill ridges amplify and hill bases de-amplify seismic waves. Development in satellite and remote sensing technologies have made digital elevation models (DEMs) freely available at high resolution, and with global cover. DEMs derived from ASTER (30m) and SRTM (90m) can therefore be utilized to model the impact of topography on seismic response. In this study, seismic waves propagation generated by 2005 Kashmir earthquake were simulated using a 3D spectral finite element code called SPECFEM3D. The ground shaking simulations and peak ground acceleration maps were generated initially assuming the homogenous ground surface and later by including the topography. Topography derived from ASTER and SRTM DEMs were simulated separately to predict the impact of DEM resolution on computed ground shaking simulations and maps. The result from model simulations shows that seismic waves are dispersed at the topographic discontinuities, leading to intensification of seismic response at some hill ridges. Comparing the simulations with and without topography also verified that the ground shaking was intensified at the hill ridges and steep slopes and has a variation of 70% greater than in the valleys, as consequences of incorporated different resolution of medium DEMs resolution. Therefore, this study demonstrated the significant impact of topography on variation of ground shaking and how seismic response modeling can benefit from the readily available global DEMs in modelling more realistic earthquake.

Keywords: ground shaking amplification, spectral-element method, ground motion, surface topography, Kashmir earthquake, Digital Elevation Model accuracy, Digital Elevation resolution

For the love of Budi Sutjahjo and Nurhasanah

Acknowledgements

I would like to thank all the following people who have been helping me in one way or in many ways during my study and MSc period at ITC:

Firstly, I would like to thank Dr. Mark van der Meijde as my supervisor who proposed interesting MSc topic and guided me through all the process with support and encouragement. Appreciation also goes out to MSc. Wim Bakker for the provoking questions and constructive criticism. To my technical advisor, Muhammad Shafique, I am grateful for his patience and assistance.

At ITC, I sincerely thank the people of AES Department who tried the best to make challenging yet exciting course; the students of AES batch 2008 – 2010 who are the family to me and the chase away my loneliness; especially for the help during thesis from Nadira Khan, Leta Megerssa, and the Spain field work team; and Tanapipat Walalite who make things at ITC always bearable.

Back home, I would to dedicate my warmest appreciation to my loving father, Budi Sutjahjo, mother, Nurhasanah, and the big family for affection and understanding who always be there for me though faraway.

Table of contents

List of figures

List of tables

List of Abbreviations

ASPRS	American Society for Photogrammetry and Remote Sensing
ASTER	Advanced Spaceborne Thermal Emission and Reflection Radiometer
CMT	Centroid MomentTensor
DEM	Digital Elevation Model
DGPS	Differential Global Positioning System
FGDC	Federal Geographic Data Committee Secretariat
GCP	Ground Control Points
GIS	Geographic Information Systems
GPS	Global Positioning System
LiDAR	Light Imaging Detection and Ranging
PGA	Peak Ground Acceleration
RAP	Red Andalusia de Positionamiento
RMSE	Root Mean Square Error
SEM	Spectral Element Method
SRTM	shuttle radar topography mission
TAF	Topographic Amplification Factor
UNISDR	United Nations International Strategy for Disaster Reduction

1. Introduction

1.1. Background studies

Earthquakes originating from deep within the earth are one of the catastrophic events that have caused and are prone to cause great damage to life and property. During the last decade, earthquakes have proven to be the most devastating natural disaster with the highest mortality rate and damage (*UNISDR*, 2006). Hence, in order to have a better understanding of this hazard's natural occurrence, it is essential to understand ground shaking characteristics along with the factors affecting them and identify factors amplifying seismic response.

Earthquake hazard is caused by a sudden release of accumulated strain through weak joints of tectonic plates i.e. faults. The stress released during an earthquake triggers seismic waves that propagate from the earthquake source to the earth's surface. Along its travelling, it is affected by source, medium and site factors which consequently govern the ground shaking at a particular site (Alexander, 1993).

At epicentres, the focal mechanism, size and directivity govern the seismic waves propagation and are identified as source effects (Allen and Gerald, 2007). Seismic waves generated during seismic source activity traverse through a medium that affect the amplitude and damping shear wave velocity of the propagating seismic waves. This process was studied using attenuation models (Anderson and Hart, 1978). Finally on the earth's surface, soil depth, topography and geology affects the ground shaking.

U.S. Geological Survey Earthquake Hazards Program has published Shakemaps, a comprehensive near-real-time ground motion and shaking intensity maps compromising the source and medium effect of seismic waves propagation (*USGS*, 2010). Although the maps are widely used for disaster preparedness, post-earthquake response and recovery, the site effects of topography on ground shaking have not been incorporated here.

One of the site factors on seismic amplification is topography which affects seismic response by the occurrence of the ground shaking amplification near the crest and de-amplifications near the toe of the slope, chiefly in the mountainous terrain area. Many preliminary methods have been applied to investigate this factor, for instance through field experiment (Davis and West, 1973), analysis of instrument records (Celebi, 1987), and field observation combined with amplification theory (Chavez-Garcia et al., 1996). On the contrary, of these findings, quantitative field measurements of topography impact on seismic amplification are difficult to obtain due to method limitation on separating amplification frequency from earthquake natural frequency (Bouckovalas and Papadimitriou, 2005).

To improve previous studies, many numerical simulations have been applied to study the terrain effects with a simple synthetic terrain, for instance by using finite element, finite differences and boundary element methods (*Geli et al.*, 1988). Most of the numerical computation methods showed how to estimate topography amplification separated from natural frequency although they were all limited by application of one dimensional step-like slopes and simplified techniques. Therefore, it was concluded that there was a need for more complex models that incorporate realistic topography. One of the methods used to improve the seismic amplification numerical model is the implementation of finite differences. Boore (1972) and Athanasopoulos (1999) showed that finite

differences in computational techniques could be used to simulate the propagation of the SH-disturbance incident on a non-planar surface. However, this method is limited by the accuracy issue, time, memory use of the computation and most of all the limited ability to incorporate surface geometries (Chaljub et al., 2007).

The advances of remote sensing technology have made Digital Elevation Model (DEM) as a representation of a real world terrain available to employ in seismic amplification modelling.
Frankel (1992) simulated the effect of topography on seismic aggravation in large scale three dimensional structures of San Jose, California . Followed this, DEMs with various resolutions and accuracies are further involved in seismic amplification modelling with various scales and intentions (Hestholm et al., 2006; Ma et al., 2007; Pitarka et al., 1998). The majority of the work previously done concentrated on the development of computational techniques for simulating ground shaking with realistic earthquake characteristics emphasizing on the accuracy of modelling calculations.

Spectral Element Method (SEM) emerged to address the numerical computation issues of more accurate computation methods, and furthermore in incorporating realistic earth models. It combines the flexibility of a finite element method with the accuracy of a spectral method and applied to various aspects of seismology (*Casarotti et al.*, 2008; *Komatitsch and Tromp*, 2002b; *Komatitsch and Vilotte*, 1998). The method was successfully demonstrated to simulate ground shaking and integrate highly diverse 3D structures, through detailed 3D terrain models (*Lee et al.*, 2008; *Lee et al.*, 2009b). These innovations drove a big advancement in seismology for a substance of ground shaking simulation incorporating more realistic earth surface terrain and earthquake source characteristics.

Though SEM have proven to illustrate accurate calculations for seismic wave propagation modelling and incorporate detailed realistic topography, only limited studies were found on emphasizing the various employed DEMs affected the model output on a regional scale. Lee (2009b) investigated the effect of topography on large-scale ground shaking simulations in northern Taiwan and recommended the use of topography on future works, although the impact of DEMs resolution on large-scale seismic amplification modelling was not studied specifically. For a small scale seismic amplification modelling, DEM resolution has been proven as a significant factor shown by comparing ground shaking amplification using fine details LiDAR DEMs and 40 m DEM (*Lee et al.*, 2009a). Only limited studies can be found regarding DEM issues on seismic amplification modelling. Shafique (2009) studied the terrain parameters for predicting topographic amplification factor (TAF) on a regional scale using geospatial tools and concluded that DEMs has measly impact on TAF. However, this study was limited by the numbers of input parameters and geospatial tools restriction on incorporating realistic earthquake characteristic. Therefore, it is still questionable of how medium resolution DEM characteristics influence regional seismic amplification modelling with realistic earthquake scenarios.

1.2. Research problem

Topography has been proven to contribute amplification in mountain ridges and de-amplification near the slope bottom, especially in area with rough terrain. Although, many numerical simulations of topographic seismic amplifications have been applied to demonstrate this, still they are limited by simplified two dimensional terrain or isolated hills and inability to incorporate realistic topography. As remote sensing technology has been advancing, numerical computations using DEMs were applied to study the seismic response amplification affected by topography. This has made a big

improvement in spite of demands for a more accurate computational method to integrate a more realistic terrain.

Specifically, SEM applied in computational seismology emerge to address the more complex computation and ability to simulate seismic wave propagation with more realistic earthquake characteristics, as well as including more detail and realistic terrain. This method has been applied successfully on large-scale and local scale area. However, majority of previous studies concentrated on the successive computational model and less were intended on how DEMs topographic attributes affect the seismic amplification modelling output. Additionally, limited studies were found on the impact of DEM on seismic wave propagation on a regional scale, specifically on the influence of medium resolution DEM characteristic on regional seismic amplification. The issue of how various DEM accuracies and resolutions influence seismic wave amplification is still a concern, particularly for seismologists and geoscientists.

1.3. Research objectives

This research was conducted to meet the following objectives:

Main objective

To assess the impact of topography on seismic amplification modelling and the impact of the accuracy of the topographic model on seismic amplification modelling

Specific objectives

1. To model the impact of topographic attributes on a simple 3D environment
2. To simulate the impact of topographic attributes on seismic amplification using SEM technique with real surface topography at regional scale
3. To determine the impact of DEM accuracy and resolution on the regional topographic seismic amplification using SEM

1.4. Research Question

Based on the preliminary result of the model utilizing simplified terrain, the simulation of seismic wave propagation will be investigated and the first two questions will be addressed:

- Can we simulate the amplification of seismic waves due to topographic attributes in a regional scale incorporating real surface topography and realistic earthquake characteristic using DEMs with various resolutions?
- Which topography attribute leads to amplification or de-amplification of seismic response?

After the simulation of seismic amplification modelling utilizing DEMs, the model performance was tested to examine the model performance influenced by different resolutions and accuracy and answer these questions:

- What is the impact of DEM resolution on regional seismic amplification modelling?
- What is the impact of DEM accuracy on regional seismic amplification modelling?

1.5. Hypotheses

Hypotheses for this research as follows:

- SEM technique can simulate seismic response amplification due to topographic effects incorporating various resolutions and topographic attributes (Komatitsch et al., 2004; Lee et al., 2009a)
- Seismic waves were amplified on the hill crests and de-amplified near the bottom of the slope.
- The predicted topographic seismic response is measly affected by the resolution and accuracy of the topographic data employed (Shafique, 2008)

1.6. Over-all Methodology

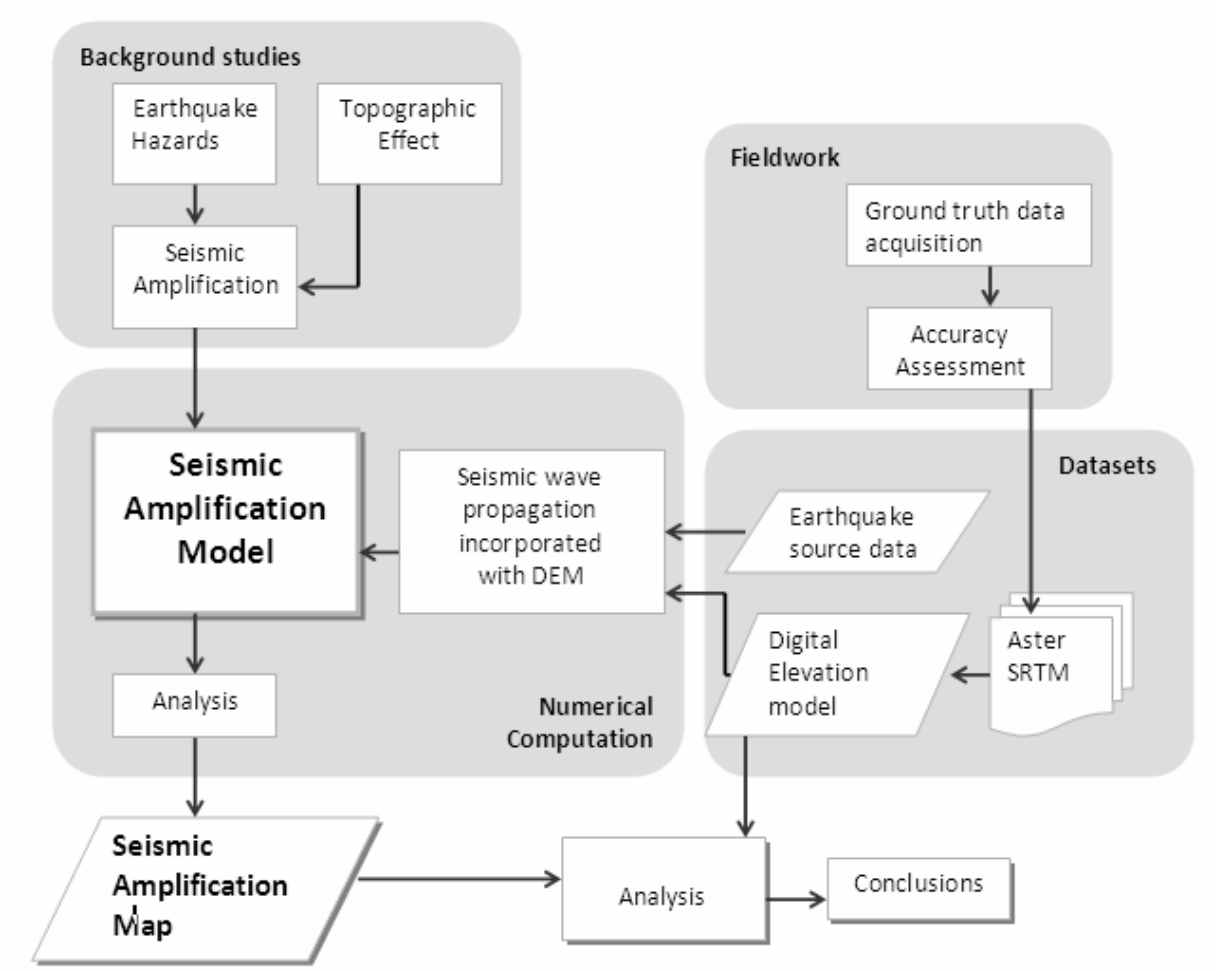

Figure 1.1 Workflow of the research, started from literature review to numerical computation incorporated DEM and complemented by DEM accuracy assessment to derive seismic amplification map. The outputs were analyzed to finally conclude the research findings.

The general workflow of this research is illustrated by the flowchart in figure 1.1. This research begins with background studies of earthquakes in general and then confines to literature review about existing studies of seismic wave modelling due to topography effects. The methodology used in this research consists of 2 parts, which are seismic amplification modelling and impact assessment of various medium resolution DEMs utilized in the model.

An accuracy assessment of SRTM, ASTER and LiDAR DEMs was conducted by obtaining ground truth data in Carboneras (Spain). 4647 points were measured using high accuracy Differential Global Positioning System (DGPS) in order to get ground truth elevation measurements, including in

various slope and aspect classes. Followed this, the RMSE (Root Mean Square Error) were calculated for each DEM.

SRTM and ASTER DEMs were utilized in our seismic amplification modelling. The model used in this research is SPECFEM3D-1.4.3 which was originally developed by Dimitri Komatitsch and Jeroen Tromp (1999). This model simulates regional seismic wave propagation based on the spectral element method for regional scale and incorporates effect of surface topography.

The model was run with 2005 Kashmir earthquake source characteristics for diverse scenario compromising DEMs with different resolutions and accuracies. The outputs of the different modelling scenarios were compared to see how topography affects the interaction of terrain derived attribute with the wave propagation on earth surface. As addressed in our research questions, the impact of DEM resolution and accuracy on derived topographic seismic response were evaluated from the modelling outputs.

1.7. Relevance

The result of the study can be extended as inputs for complete seismic wave propagation modelling with realistic earthquake characteristics in incorporating sufficient terrain model and terrain derived attributes at the regional scale. The study can be beneficial for understanding the impact of terrain derived attributes on seismic response and various DEM resolution influences of seismic wave interaction at the earth's surface. Furthermore, this research can motivate the existing regional ground shaking modelling to improve the simulation with the importance of site effects, especially topography.

2. Literature Review

Pakistan has suffered great loss of life and damage due to earthquake disasters (*USGS*, 2009). This condition occurs because of the Kashmir complex tectonic setting where the eastern Himalayan syntaxes are formed by the east west trending India-Eurasia plate and north south trending India-Burma plate margins (*Rao et al.*, 2006). The setting triggers the mechanical interaction between plates, such as collision, friction, and separation that accumulates strain energy which ultimately leads to rupture, and thus, earthquake (*Towhata*, 2008).

A devastating earthquake occurred 95 km Islamabad, Pakistan at 9.50 pm (local time) on 7th of October 2005 with magnitude 7 and caused the heaviest damage in the Muzaffarabad area, Kashmir (USGS, 2005). Most of the damage in this area was associated to the ground shaking as the most significant primary impact of earthquake hazard (*Murck et al.*, 1997). In Kashmir case, ground shaking distribution was concentrated along the strike of Kashmir thrust due to the rupture directivity (*Ali et al.*, 2009).

Additionally, Kashmir located in a region with large varying topography with steep slope and thickly soils covering the valleys. This condition is believed as an ideal condition for ground shaking amplification (*Erdik and Durukal*, 2004). Topographical impact in ground shaking amplifying has been observed from the past earthquakes and investigated by instrument records. The field measurement show that there were strong effect of topography creating amplification on hills and slopes (*Celebi*, 1987; *Davis and West*, 1973).

2.1. Topographic factors on ground shaking amplification

It is well established that topographical effect on ground shaking occurs due to the characteristic of seismic wave interaction with diverse material. Waves travel within medium with varying physical and affected at the transition (*Erdik and Durukal*, 2004). Some of the processes related to this material interaction are discussed as follow:

2.1.1. Refraction, reflection and critical angle

The different layer materials interact with the waves and initiate reflection or refraction or both (*Lowrie*, 2007). Furthermore, it is explained that reflection occurs when the angle of wave path is altered in the same angle after it arrives at different material to the direction of its arrival. The angle between the normal to the interface and the normal to the incident wave front is called the angle of incident (i), while the angle between the normal to the interface and the normal to the reflected wave front is called the angle of reflection (i'). In Figure 2.1 the law of reflection which applies to the angle of reflection is equal to the angle of incident (i=i'). The interaction between the angle of incident can be extended to cover part of the disturbance that travels into the second medium with different material (n_2) and velocity (v) as seen in Figure 2.2. The relation proportional between the two is explained by Snell's law as equation (1) below:

$$\frac{\sin i}{\sin i'} = \frac{n_1}{n_2} = \frac{v_1}{v_2} \qquad (1)$$

If the wave velocity in layer 2 is greater than the wave velocity in layer 1, the angle of refraction is greater than the angle of incident. Snell called this phenomenon as critical refraction.

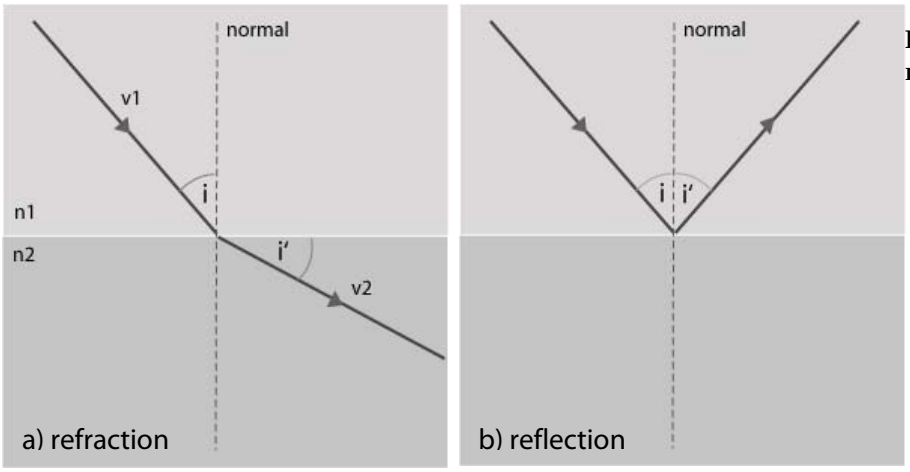

Figure 2.1 Refraction and reflection of seismic waves

2.1.2. Focus and defocusing

The focus and defocusing of seismic waves depend on the curved terrain. Generally, seismic waves are trapped on the convex and scattered by concave shape of topographic features, shown by figure 2.2 (*Lay and Wallace*, 1995). These processes cause trapping seismic wave in the top of convex terrain attribute and damping in the foot of concave features.

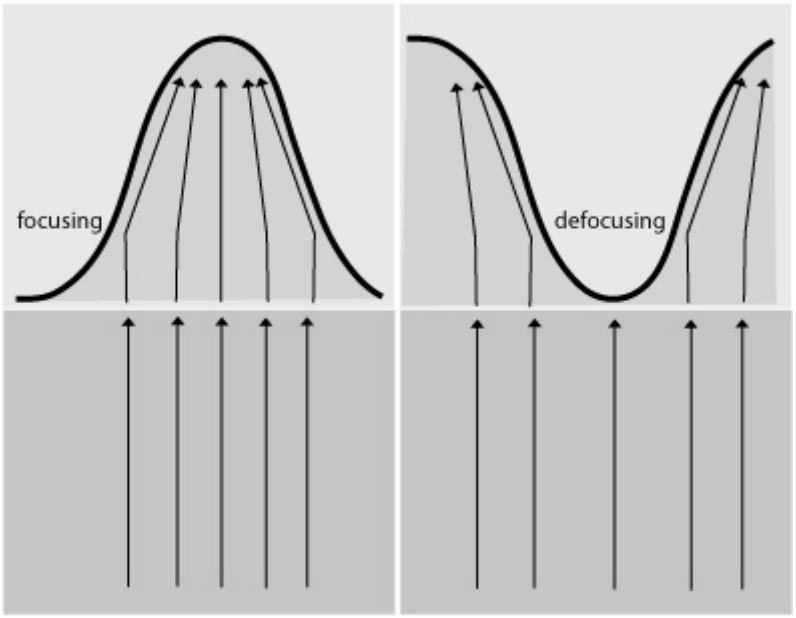

Figure 2.2 Focusing (a) and defocusing (b) effect of material interaction to seismic waves response

2.1.3. Material interaction of terrain attributes

Various terrain attributes create different slope degrees, slope angles and directions, and in combination form a complex system of isolated hills and basins. The variety of the terrain attributes alter the direction of propagating seismic waves taking into account material process interactions and

resulting topographic effects on seismic response. Specific terrain features affected seismic wave propagation response on creating amplification or attenuation (*Erdik and Durukal*, 2004).

Slope inclination is believed to be the most sensitive feature of site response because it determines the angle of reflection and diffraction of seismic waves (*Boore*, 1973). Steep slope tends to pack and focus the reflected seismic waves at the slope crest, while gentle slopes scatter the diffracted seismic wave, as can be seen in Figure 2.3.a. and Figure 2.3.b. The effect of varying slope angles was investigated by numerical model and reported that with the increasing slope angle, the magnitude of the amplification at the peak increased and varied about 15% - 25% (*Ashford et al.*, 1997).

The relationship between slope aspect and the seismic wave propagation determined the location of high amplification. Inclined waves are amplified for waves travelling into the slope and de-amplified for waves travelling away from the slope. This amplification of inclined wave is a factor of 2 larger than for a vertically propagating waves (*Ashford and Sitar*, 1997). Effect of slope aspect is illustrated by Figure 2.3.c.

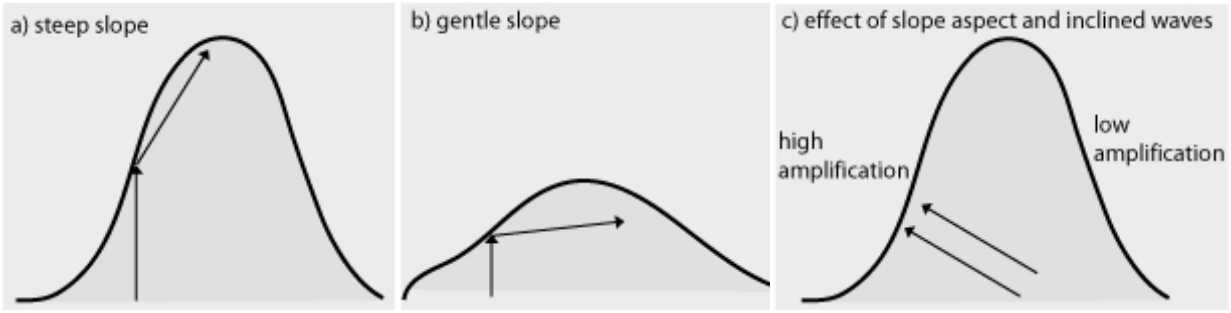

Figure 2.3 Terrain attributes factors on seismic response, a) steep slope, b) gentle slope, c) slope aspect

This topographic effect has been proven by many studies. Ridges and top of the hills cause amplification while valleys and hill bases tend to attenuate seismic response. Studies on the San Fernando earthquake revealed that a zone depression was found at the bottom and 30 to 50% amplification took place near the top (*Bouchon*, 1973). A recent study of three-dimensional realistic topography at local-scale of Taiwan has proven that amplification at the crest varied from a factor of 2 and vice versa in the valley (*Lee et al.*, 2009a).

2.2. Topographical impact on seismic amplification modelling studies

Preliminary studies of topographical impact on seismic amplification were carried out by means of field measurement and analysis of instrument records. An analysis from accelerogram records showed that the amplification from the hill response was expected 25 to 50% higher than a flat surface (*Boore*, 1973). Studies on Chile earthquake was conducted using dense arrays of seismogram after the main event and the analysis of extensive data reveal that there was substantial amplification of seismic response on the ridges (*Celebi*, 1987). However, these previous methods were limited by inability to quantity the amplification and the simplified two dimensional terrain model.

The advances of computer technology and geo-science computation have made many numerical modelling codes available to be applied in earthquake phenomenon research. Various computing technique have been more frequently employed to formulate conceptual models and mathematical analysis in many fields (*Jing*, 2003). The advancement also was applied in topographical effect studies on ground shaking studies. Geli (1988) has reviewed some of the preliminary methods, ranging from finite element, finite differences, integral equation method and boundary method by comparing them with theoretical background of seismic amplification. In summary, all the

computational techniques show a significant amplification at hill tops and complex pattern of seismic wave on the hill sides. The limitation from previous works was the failure to include complex two-dimensional structure. Therefore, there was a need for taking into account more complex method to deal with subsurface layering and neighbouring ridges.

One of the methods that very common and mainstream used is finite differences. The advantages of finite differences are the ability to handle material inhomogenity, non linearity and the availability of well-verified computational codes for large or small scale problems. For geo-science computation, Pitarka (1999) has proved the validation of this method for seismic motion simulation. The finite differences method was applied on investigating the effect topography on base motion in Egion, Greek based on a simple 2D profiles. The numerical computation results showed that amplification existed close to the crest of steep slope and confirmed this from accelerograph records (*Athanasopoulos et al.*, 1999). Although the result was as expected, still the research was limited by step-like terrain which is not a complete representative of real world topography.

In the 1990's three dimensional models started to develop and were utilized in topographical impact on seismic response. Hestholm (1999) carried out a 3D finite differences model of seismic scattering in large scale area incorporating free surface topography of synthetic parabolic hills. Followed this, 3 x 3 km aperture NORESS topographic data was employed in the model using the same numerical techniques. Ripperger (2003) applied finite differences to simulate seismic motion induced by Merapi volcano activity with the fine spacing grid of 15 m. The combination of finite differences computation techniques and DEM utilization was a big improvement in realistic seismic amplification. However, the finite differences method was limited by the long computation time and more accurate computational techniques were suggested adequate to integrate fine detailed DEMs with precise calculations.

2.2.1. Spectral element method (SEM) on seismology computation

An improvement with respect to the finite difference approach came up from the demand for accurate calculations and the use of realistic earth models. The method used was called the spectral element method (SEM) which combines the flexibility of a finite differences method with the accuracy of a spectral method SEM. It adopted the basic theory of computational fluid dynamics to simulate seismic waves and since then it has been applied in various aspects of seismology, for instances in complex geological media (*Casarotti et al.*, 2008), global seismic wave propagation (*Komatitsch et al.*, 2002) and investigating basin effect on seismic motion (*Delavaud et al.*, 2006).

Komatitsch (1999) defined the modelling environment of SEM as a finite earth model shown by Figure 2.4. The displacement field of earth was determined by an earthquake in a finite earth model as shown. This volume model was bordered by a stress-free surface $\delta\Omega$ and absorbing boundary Γ. Xs is the earthquake source that triggers a seismic wave and this artificial epicentre can be placed anywhere inside the volume block. The free surface $\delta\Omega$ reflects seismic wave and ideally the artificial boundaries absorb this seismic wave. This boundary condition is appropriate for simulating topographic effects on seismic amplification because the vertical sides absorb the seismic wave and the free surface reflect and refract as it interacts with seismic wave.

Figure 2.4 Finite model earth of SEM. On the sides and bottom it uses absorbing boundary and on the top it uses a free surface boundary.

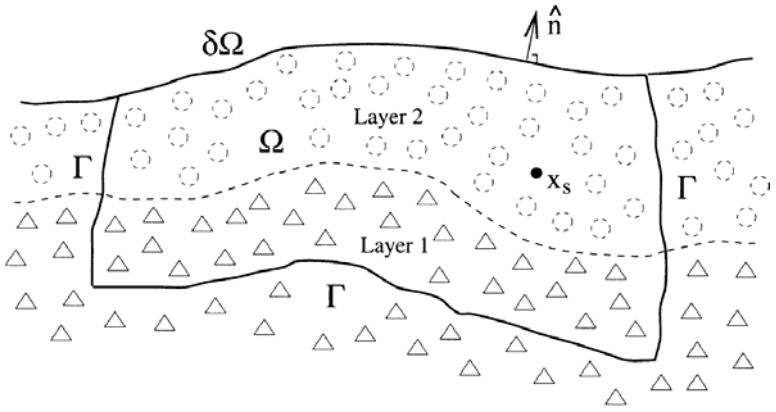

Recently, SEM techniques on computational seismology were extensively improved and developed. The computational technique was validated to simulate global seismic wave propagation including the effect of oceans, rotation and self-gravitation (*Komatitsch and Tromp*, 2002a; *Komatitsch and Tromp*, 2002b). Following this, the global seismology simulation was applied in three-dimensional inhomogenous earth model with deformed geometry (*Chaljub et al.*, 2007). The computational code also has been made available as the SPECFEM software package by Computational Infrastructure of Geodynamic as part of GeoWall consortium (*Geodynamics*, 2009).

CIG has developed and published a number of model types ranging from regional wave simulation in 1 Dimensional surface (SPECFEM1D Version 1.0.0), regional wave simulation in 2 dimensional environments (SPECFEM2D Version 5.2.2), wave simulation in 3 dimensional basins (SPECFEM3D Version 1.4) and global simulation of wave propagation in entire earth (SPECFEM3D Globe Version 4.0.3).

In general, SPECFEM packages offer simulation of seismic propagation in various environments. The simulation also includes effects due to lateral variations in compressional-wave speed, shear-wave speed, density, a 3-D crustal model, ellipticity, wave propagation characteristic in the oceans, rotation, self-gravitation and topography as well as bathymetry.

2.2.2. SPECFEM Simulation – input, mesh and output

Mainly SPECFEM required earthquake source characteristics to simulate seismic wave propagation. This source characteristic is summarized by CMT Solution file which is an earthquake event file based on centroid moment tensor methods of earthquake focal mechanism. CMT solution files from past earthquakes can be downloaded from the CMT website (*CMT*, 2006). Optionally, topography or bathymetry or both can be taken into account into the simulation. The complete processes of SPECFEM input processing is explained in Appendix D.

The mesh design is a critical step in any method based upon a mesh of elements (*Komatitsch and Tromp*, 1999). For the computations purpose, the finite earth model as shown in Figure 2.4 is divided into curved elements, quadrangles in two dimensions and hexahedra in 3 dimensions. This hexahedra shape furthermore complicates the computation but it is required to ensure the number of grid points per wavelength is sufficient in addressing the seismic wave computational problem.

To deal with the problem of complicated computation, the volume block is divided into two layered-cake models by one or more buffered layers. This layered model is constructed with coarser mesh at the bottom to adopt the seismic wave that generally increased with depth. The finer mesh at the surface and unevenly shape of each element in volume model have proven to give a satisfying results. High-resolution mesh reduces the amount of numerical dispersions and anisotropy and thus it

is crucial for accurate result (*Komatitsch et al.*, 2002). An example of a complete mesh is shown by Figure 2.5.

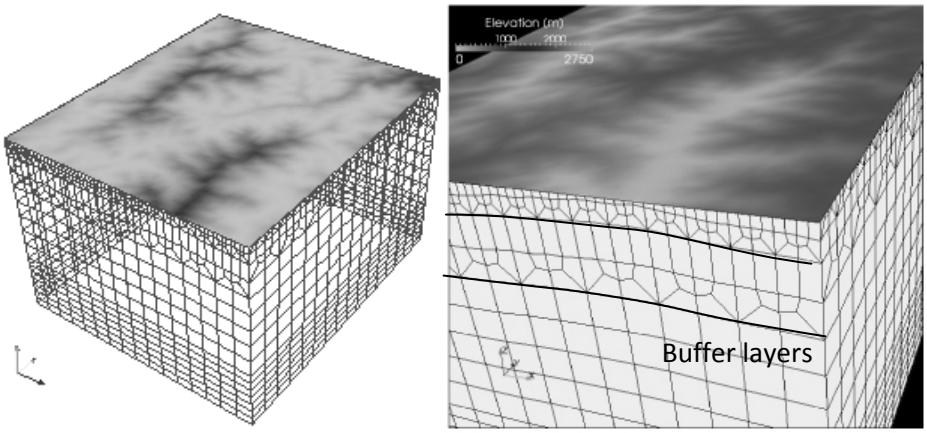

Figure 2.5 SPECFEM mesh example, left: a complete mesh, right: two different grid sizes near the mesh surface and buffer layers.

There are several options of SPECFEM outputs according to observation needs. The general output is the recording of seismic wave amplitude and can be documented for each time step. SPECFEM generates shaking maps that are obtained after the simulation is finished. This set contains map of acceleration, velocity and displacement. SPECFEM is also able to perform accurate synthetic seismogram records according to the desired location.

2.2.3. SPECFEM3D performance

From the theoretical and numerical point of view, the SPECFEM3D simulates seismic wave propagation simulation without limit of frequency content. It is possible to integrate highly diverse 3D structures through a realistic DEM of the earth's surface as an input in the program. Several studies have been carried out combining the spectral method with realistic topography and show more detail and realistic seismic wave simulations for instance the a large-scale study on ground shaking amplification on Taipei basin (*Lee et al.*, 2008) as well as the study conducted in Yamingshan incorporating realistic topography (*Lee et al.*, 2009a).

Although the previous studies showed the practical use of SPECFEM software, the number of researches which have been utilizing the package are still limited. Therefore, this package has not been tested on many diverse environments, hence various resolution of DEMs or study area.

2.3. DEM issue on seismic amplification numerical modelling

The advances of geo-science computation combined with remote sensing technology have made possible the modelling of topographic ground shaking amplification using DEMs. The employed DEM derived attributes in seismic amplification modelling is influenced by specific DEM characteristics (*Shafique et al.*, 2009). Therefore, it is indeed worthy to study DEM characteristics and how these specific characteristics of DEMs affect the modelling output.

Nowadays, remote sensing techniques are common in obtaining DEMs. Scientists and cartographers have been developing DEMs with higher and more accurate DEMs to answer the needs to apply DEM in more detailed applications. Users now have more choices to decide which DEMs suit best to meet their objectives. The scope of options ranges from high resolution DEMs with up to 2 meters resolution such as LiDAR, IKONOS, or Quickbird, to medium to coarse resolution DEMs such as ASTER, SRTM, and GTOPO with resolution from 30, 90m to 1 km respectively. The high resolution is more likely used for detailed application while the medium to coarse resolution DEMs are often applied for global or continental scale implemention and analysis (*Li et al.*, 2005).

2.3.1. DEM accuracy

Accuracy of DEM is commonly referred to as the closeness of an estimated elevation to a standard or accepted correct value and important not only for producers but also for users (*Li et al.*, 2005). Therefore, it is important to assess DEM accuracy before computing its derivatives or involving them in further terrain analysis and modelling.

Amongst other accuracy assessment methods, the best way to map terrain's features with high accuracy is provided by using GPS (*Gorokhovich and Voustianiouk*, 2006; *Lunetta et al.*, 1991), especially for SRTM accuracy assessment (*E. Rodríguez and J.M. Martin*, 2003). Utilization of GPS in accuracy assessment also meet several guidelines of national mapping agencies (*ASPRS*, 2004; *FGDC*, 1998). Therefore, accuracy assessment technique using GPS needs instrumentation with high accuracy capability for acquiring good quality ground truth data. The instrumentation is made possible by the advancement of differential GPS which can obtain less than 3 cm accuracy comparatively to recent generation of DEMs with 2m resolution (*Leica Geosystems*, 2004)

The Root Mean Square Error (RMSE) often follows the measurement as a statistical computation of accuracy assessment. This calculation technique has been widely applied to DEM accuracy assessment (*Aguilar et al.*, 2007; *Gorokhovich and Voustianiouk*, 2006; *Mockton*, 1994) for any kind of resolution. Theoretically, Figure 2.6 explains how root mean square error is computed (*Li*, 1988).

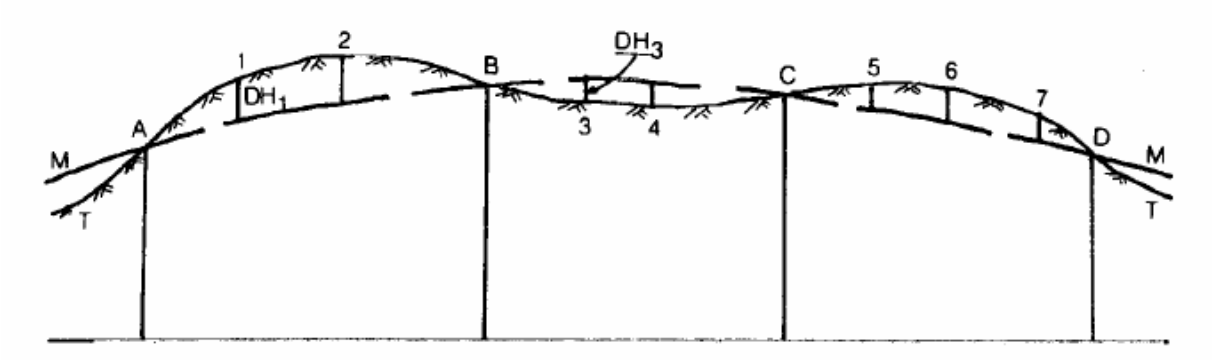

Figure 2.6 The differences between real world and terrain data as calculated by RMSE (Copied from Li, 1988)

In Figure 2.6, we can see T as a terrain surface and M as mathematical function which constructed point A, B, C, and D. The height difference between M and T are DH1, DH2,…, DHT. RMSE is computed by inserting DHi and N (number of points) in the equation (2) below:

$$RMSE = \sqrt{\frac{\left(DH_i^{\,2}\right)}{N}} \qquad (2)$$

Although Li (1988) suggested to measure the dispersion, the RMSE is the simplest yet widely method applied anywhere due to its value being constant or spatially stationary over the study area (*Castrignanò*, 2006). RMSE calculation for DEMs accuracy assessment is also a requirement to meet mapping standards of national mapping agency such as FGDC (1998) and ASPRS (2004).

Specific DEMs congregate errors from certain resources and processes. Likewise is SRTM DEMs who has a standard linear vertical absolute height error of 16m and relative vertical error of 20 meters (E. Rodríguez and J.M. Martin, 2003). The largest error contribution of 10 meters comes from roll angle firings and the smallest of 0.5 meter comes from motion aliasing (Rabus et al., 2003). A research of SRTM accuracy assessment in US and Thailand conducted by CGIAR resulted SRTM errors ranged from 7.58+-0.60 meters in Phuket, Thailand and 4.07+-0.47m in Catskills, US. Another important conclusion is, this error is correlated with slope more than 10 degrees and certain aspect values (Gorokhovich and Voustianiouk, 2006).

ASTER DEMs vertical accuracy was validated by survey using GPS obtaining up to 13000 ground control points in US and 300 GCPs in Japan. This survey resulted in a20m at 95% confidence accuracy for ASTER GDEM global basis(ASTER GDEM, 2009). The primary conclusion by this research was that ASTER suffers error from two primary sources. The first error comes from residual clouds in the ASTER scenes for generating ASTER GDEM, and the second error comes from algorithms used to generate the final GDEM. An addition 10% error is caused by a stripping effect of poor calibration of CCD (Toutin, 2008).

In general, the denser and the higher resolution terrain data are, the more accurate the DEMs product will be and it is the same case for LiDAR whose data accuracy and density are exceptionally high and reliable. Liu (2007) applied data density research to improve LiDAR accuracy assessment and show that LiDAR data can be reduced to particular level without a substantial accuracy of output DEM which will affect the computation time using LiDAR DEMs. The complete guide for assessing LiDAR accuracy was published by ASPRS(ASPRS, 2004) and according to this LiDAR accuracy value is 1.96*RMSE.

2.4. DEM impact in seismic amplification modelling studies

Although there have been numerous studies of topographical effects on seismic amplification, most of the studies are emphasizing the ability of the computation technique to simulate more realistic earthquakes. Only few of the research investigating the DEM characteristic interference on seismic amplification output, especially on a regional scale

Shafique (2008) have applied geospatial tools for predicting the seismic amplification, and emphasizing on the influence of DEM derived attributes from a variety of DEM accuracy and resolution in Kashmir earthquake. It was concluded that DEM resolution and inherent errors have little significance to topography. However, the geospatial method here is limited by few input parameters of the model.

The recent research done by Lee (2009b) incorporated a LiDAR DEM with 2m resolution to study the effect of realistic surface topography in Yangminshan, Taiwan and proved that on the local scale high resolution imagery was sufficient to calculate the seismic waves. High resolution DEMs is suitable to apply in a local scale because it takes into account all the detail, but the difference of resolution has not been tested yet on a regional scale.

3. Methodology

3.1. Study area

Regional seismic amplification modelling was applied in order to investigate the effect of terrain attributes on Kashmir region. It is located in the north eastern region of Pakistan and its east frontier is bordered by India. The biggest city is Muzaffarabad where the largest number of fatalities of 2005 earthquake happened. Kashmir has a large varying terrain which makes it a very interesting study for topographic seismic amplification studies. The elevation heights vary from the mean 707 to an extremely high mountain of 2750 meters as a part of the Himalayan foothill. The map of Kashmir is shown by Figure 3.1.

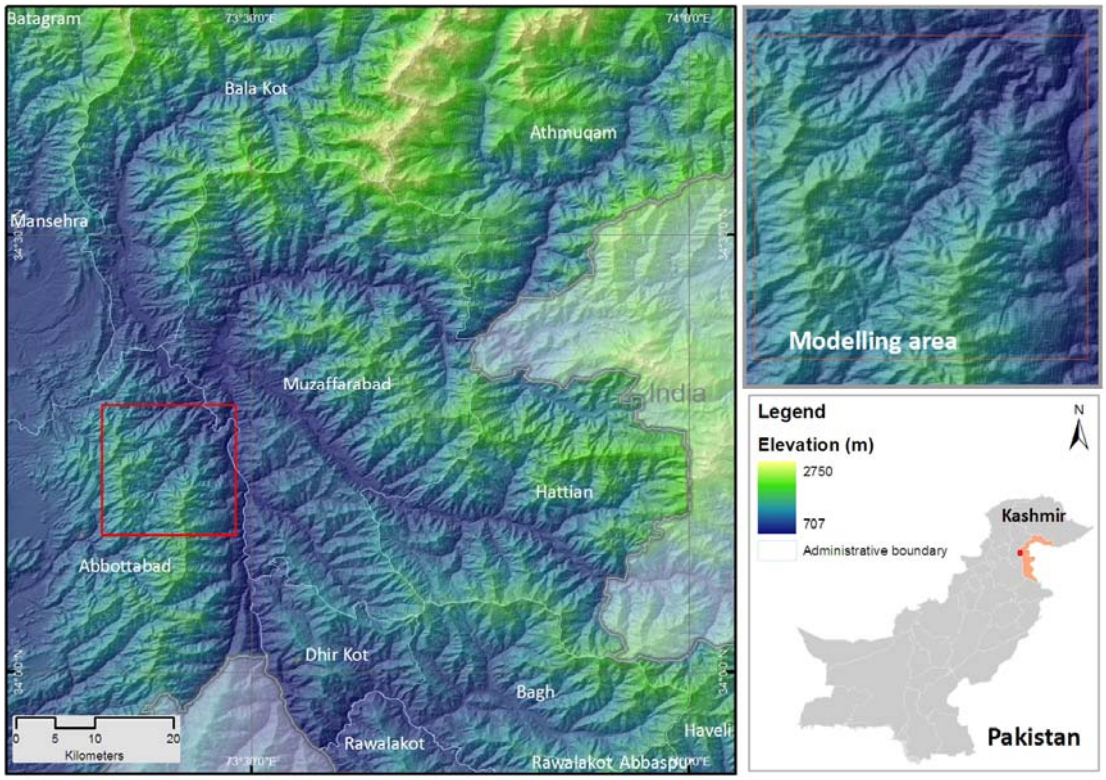

Figure 3.1 Map of Kashmir and modelling area

3.2. General simulation flow

Topographic seismic amplification modelling was investigated by means of numerical computation based on spectral element methods. Here we used SPECFEM3D-1.4.3 software package (see Chapter 2.2.2 and 2.2.3) developed by Komatitsch (1999). Additionally, some of the analysis was completed using GIS and visualization software. SPECFEMD complementary manual is shown in Appendix C.

Seismic amplification simulations were conducted based on a workflow as shown by Figure 3.2. It started with model parameterization and data processing, including DEM accuracy assessment

then followed by mesh creation and simulation. Finally, the outputs from the model were visualized and analyzed. Each block of the flowchart was discussed in following sub-chapters.

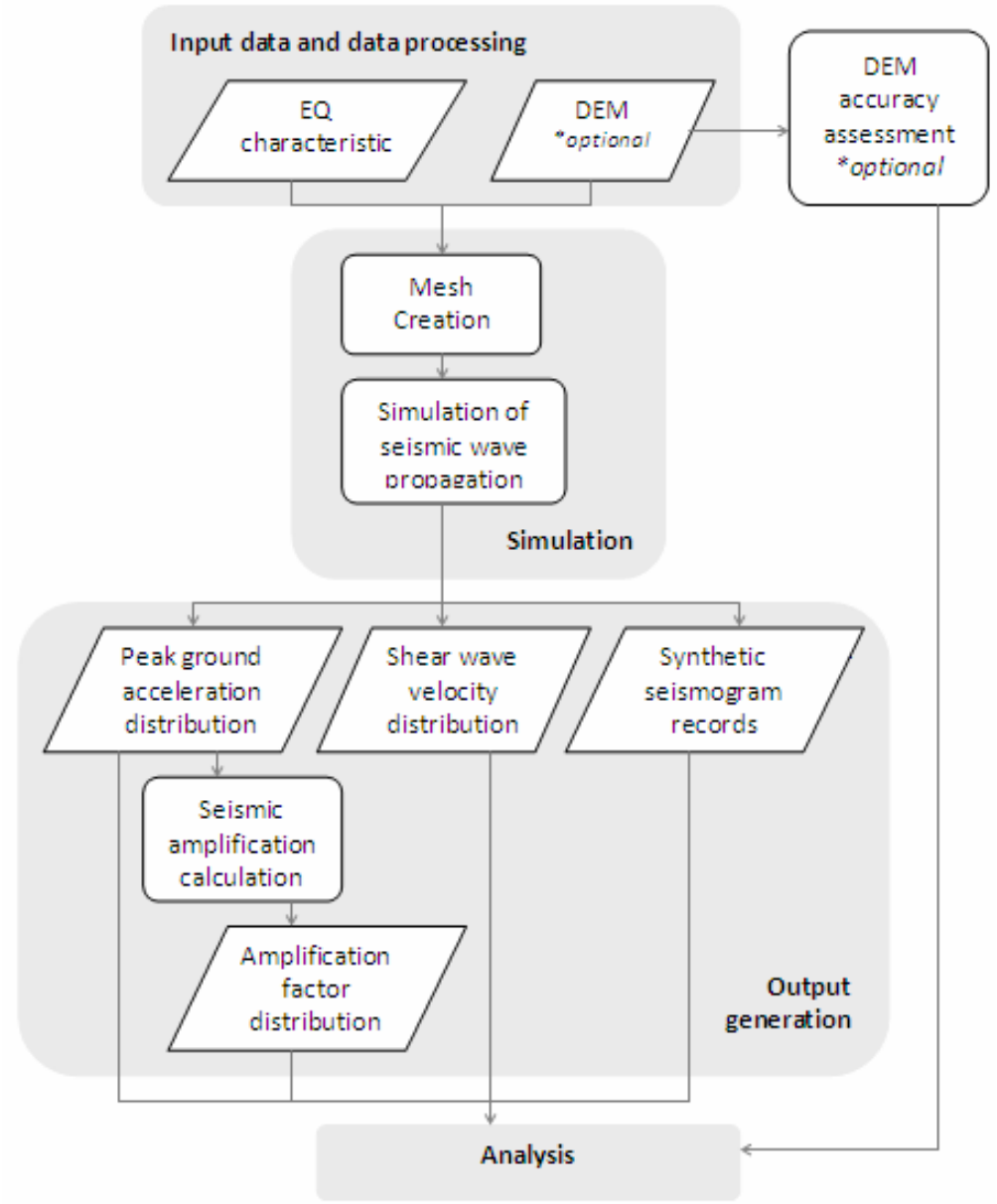

Figure 3.2 General simulation work flow from input data and data processing including accuracy assessment, simulation, output to analysis.

3.3. Model parameterization and input data processing

This sub-chapter explains model parameterization, data acquisition and data processing procedures that needed to be prepared before the simulation.

3.3.1. Model parameterization and mesh design

7 November 2005 Kashmir earthquake source characteristics were applied in this modelling. The earthquake was 7 magnitude and the epicenter were located on 73.408 E and 34.243 N, in the depth of 26 km. To include this earthquake source characteristic we applied CMT Solution information downloaded from CMT website (www.globalcmt.org). CMT file was adjusted into 13

lines ascii files to match the model requirement. Exampe of CMT Solution of Kashmir is shown in Appendix B.

The same mesh design parameters were implemented for each simulation scenario, shown by Table 3.1 and the mesh example is shown by Figure 3.3. The size of the mesh is 14.5 x 14 km with the depth of 40 km. Two buffer layers were applied in to dampen mesh distortion due to steep topography. The ASTER and SRTM DEMs were resampled according to the mesh resolution and subsequently preserved at the top of mesh block. Each simulation scenario was performed with 0.011 time step, and the total duration of the simulation is 73 minutes, that is 6700 timesteps. The complete parameter file is shown in Appendix A.

Size	: 14.5 x 14. 5 km
Depth	: 40 km
Epicenter location	: 26 km
Depth of epicenter	: 73.408 E, 34, 243 N
Doubling	: 2 layers
Time step	: 0.011 second
Time step amount	: 6700 time step
Total duration	: 73 minutes

Table 3.1 Model parameters

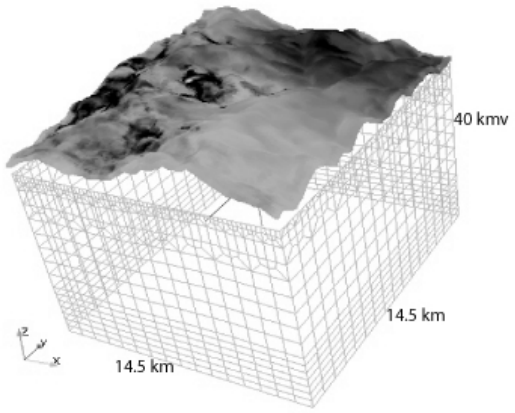

Figure 3.3 Mesh design, 14.5 x 14.5 km with 40 km depth

3.3.2. DEM Acquisition

For both simulation and accuracy assessment, we obtained DEM based on the sources on Table 3.2.

Purposes	DEM	Sources	Acquired date	Resolution
Seismic amplification modelling	SRTM	http://www2.jpl.nasa.gov/srtm	September 2009	90 m
	ASTER	http://asterweb.jpl.nasa.gov/gdem.as	September 2009	30 m
Accuracy Assessment	SRTM	http://www2.jpl.nasa.gov/srtm	August 2009	90 m
	ASTER	http://asterweb.jpl.nasa.gov/gdem.as	August 2009	30 m
	LiDAR	ITC	2007	2 m

Table 3.2 DEMs acquisition data, both for seismic amplification and accuracy assessment.

3.3.3. DEM accuracy assessment

An accuracy assessment of SRTM and ASTER DEMs was conducted in order to investigate the DEMs inherent error. The accuracy assessment was carried out in Carboneras, Spain (Figure 3.4) by obtaining 5000 GCPs of elevation to calculate vertical accuracy of DEM.

The GCPs were collected on accessible profiles on top of various slope and aspect classes to see the variety accuracy between steep slopes and flat surfaces.

3.3.3.1. Instrumentation

We used Differential Global Positioning System to collect selected points using LEICA GPS 1200 instrument. The device is capable to achieve 10 mm on horizontal accuracy and 20 mm for vertical accuracy, although its performance and accuracy is subjected to the number of available satellites, satellite geometry, observation time, and ionosphere condition.

Leica GPS1200 consists of a dish antenna mounted to a pole for obtaining satellite signal and a remote interface attached to set up and monitor the measurement. It also equipped with SmartTrack technology which is able to acquire all visible satellites within seconds.

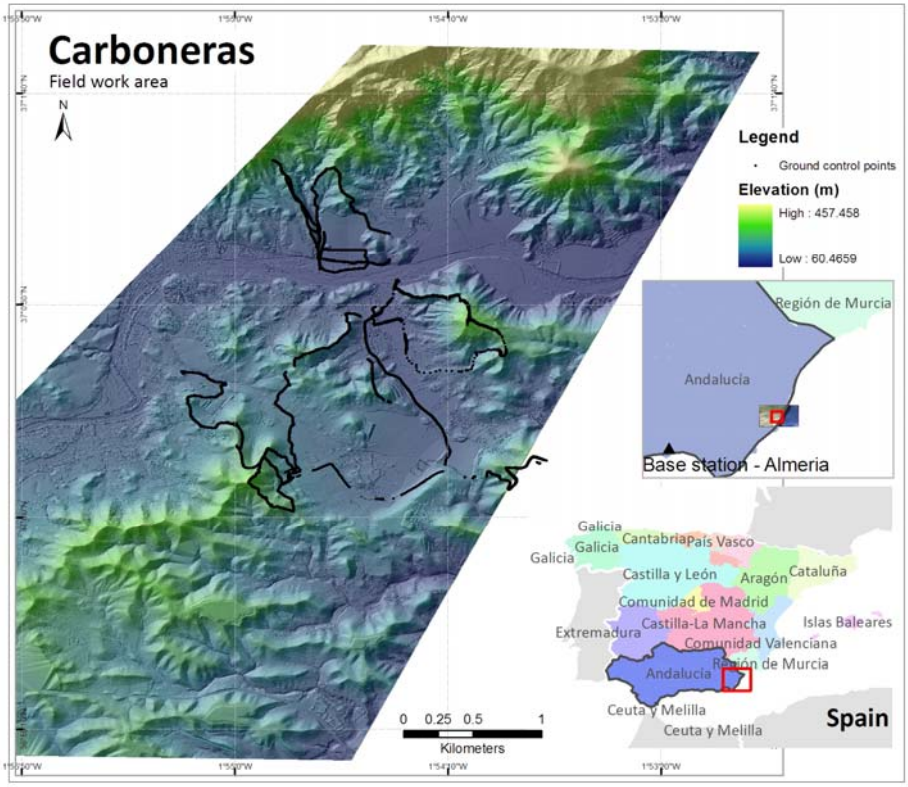

Figure 3.4 Map of accuracy assessment area with location of ground control points and base station location.

3.3.3.2. Data acquisition and post-processing

During two weeks, measurements were taken within a 2 week period on more than 20 profiles to cover various slope and aspect classes using DGPS instruments. Up to 5000 points were collected as shown in Figure 3.4. The DGPS was set up to automatically collect elevation measurements in every 1 meter interval along the profiles. According to satellite availability, instant measurements ranged between 1m to 3m accuracy for horizontal accuracy, and 3 to 9 m for vertical accuracy. All the point height measurements were downloaded daily from the instrument to the computer using Leica Geo Office. Subsequently, these points were mapped to evaluate the fieldwork and to make the next day field work plan.

The data collected in the field was subsequently post-processed using base station data provided by base station network called Red Andalusia de Positionamiento (RAP). RAP has numerous base stations scattered all over Spain and each records base station data continuously for 24 hours a day. The closest base station for this fieldwork area was located in Almeria, 50 km from Carboneras (Figure 3.4).

For this study, the daily differential correction RINEX data was selected accordingly and downloaded from the RAP website. Field measurements were post-processed using a differential correction within the Leica Geo Office software package and then plotted on the map.

3.3.3.3. RMSE calculation and statistical analysis

After differential correction was carried out profiles from, field measurements were taken for statistical analysis. This profile was overlaid with LiDAR, ASTER and SRTM DEMs, then all the corresponding values were extracted using ArcGIS.

In order to observe the trend line, data from DGPS and DEMs were plotted in a graph with elevation in meter as y axis. Data disparity were calculated and plotted in a graph as well. Following this, RMSE (see Chapter 2.3.2) from each DEM was calculated and plotted in a scatter-plot graph.

For investigating the accuracy assessment on slope terrain, the general data were divided into two groups. The first group consists of measurements on relatively flat surfaces with less than 10 degrees slope and the second group contains measurements on sloped terrain with more than 10 degrees slope. RMSE between DGPS and DEM data for each group were calculated and compared. DGPS and DEM for each slope classes were also plotted on scatter graphs. The statistical analysis was done using R software.

3.3.4. DEM processing

DEMs utilized in seismic amplification modelling were downloaded in a ready-to-use format for GIS packages. This file format needs to be processed and the coordinate system were adjusted to WGS1984 according to SPECFEM3D requirements. DEMs were clipped to the study area extent then converted into ASCII Format file. These steps of DEMs processing were completed using ArcGIS and the complete process flow is shown by Figure 3.5.

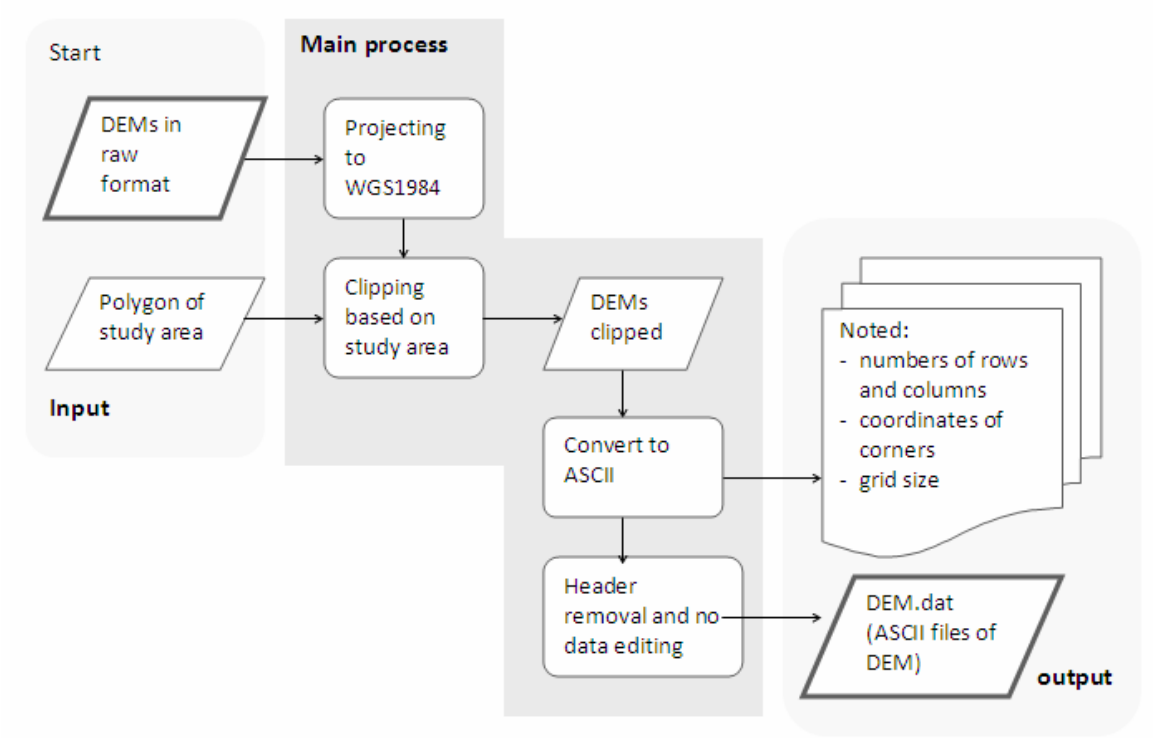

Figure 3.5 Data processing workflow from DEMs imageries to DEM ASCII file format

3.4. Mesh and simulation scenario

In this study, SPECFEM3D-1.4.3 was applied to simulate the seismic wave amplification. This package is specifically designed for regional or local scale seismic wave propagation. The code was written in Fortran95 language and the simulation was completed under Linux operational system.

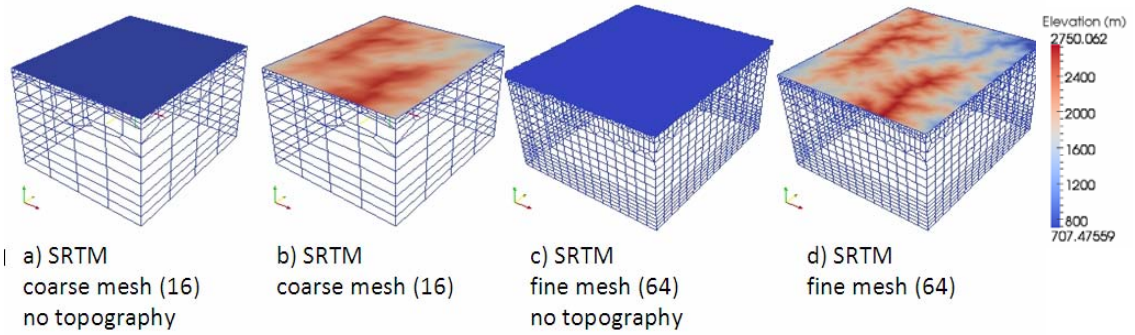

Figure 3.6 Examples of SRTM mesh scenario from: a) SRTM 16 without topography, b) SRTM 16, c) SRTM 64 without topography and d) SRTM 64

Two type of mesh resolutions were implemented in the simulation, coarse mesh 16 x 16 and fine mesh 64 x 64. This consideration was taken in order to observe the effect of different mesh resolutions on computations. Examples of SRTM meshes are shown in Figure 3.6. It is clearly demonstrated the various grid computations present by volume block geometries. The elevation of the topography is presented in gradual red to blue colour scale, where deep red is the highest elevation and deep blue is the lowest elevation.

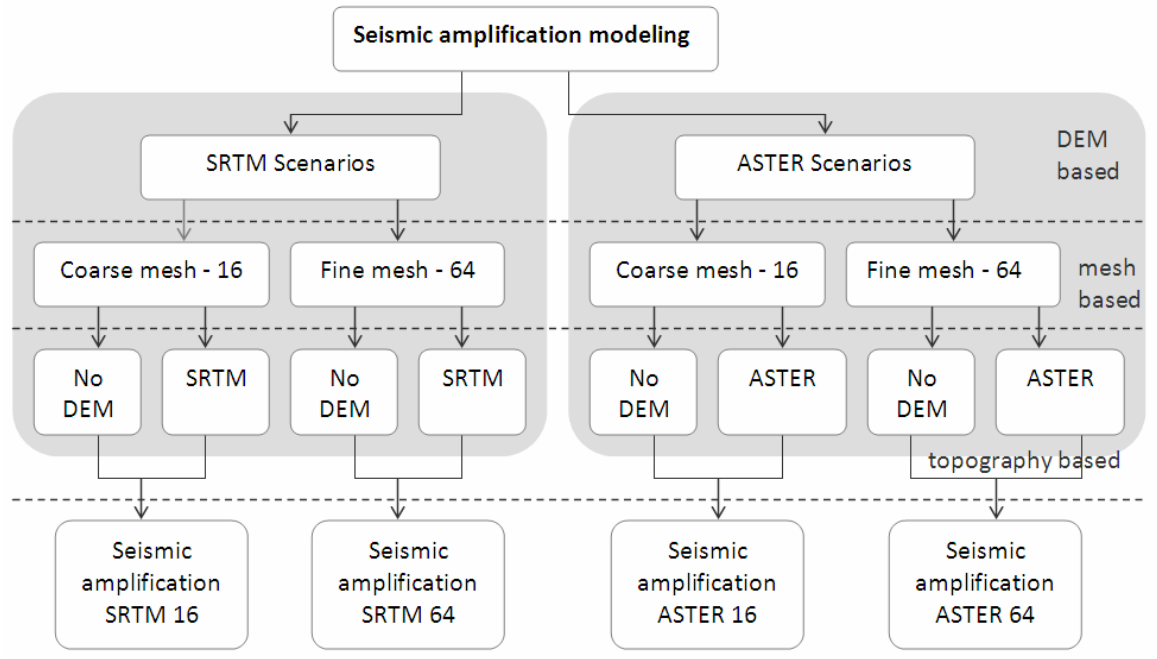

Figure 3.7 Seismic amplification simulation scenario tress, based on DEM, mesh and topography

In order to investigate the effect of topography on seismic amplification in Kashmir, we complemented each DEM incorporated simulation with an excluded topography simulation. Each simulation was composed as a pair of coarse mesh (16 x 16 grids) and fine mesh (64 x 64 grids) to consider the effect of mesh resolution. Additionaly, each model was simulated with SRTM and

ASTER to assess the effect of various DEM resolutions as illustrated by Figure 3.6. The complete mesh and scenario parameters are noted in.

3.5. Output generation

Model outputs can be viewed either in ParaView software or OpenDX. In this research, ParaView is frequently used for output visualization. SPECFEM3D also generates output in ASCII files contains longitude, latitude and output value which can be easily plotted in GIS software for further analysis.

For each scenario, the outputs were generated as follows:

- Shear wave velocity distribution every 50 time steps

  In order to observe the wave propagation pattern, records of shear wave velocity in every 50 time step of simulations are stored in the folders. These series of maps can be viewed as animation showing the propagation of seismic waves in the study area using ParaView or OpenDX as visualization software package.

- Peak ground acceleration distribution

  Peak ground acceleration distribution were generated in ASCII files then plotted with ArcGIS to observe the peak ground acceleration pattern and derive seismic amplification distribution.

- Amplification maps

  SPECFEM3D does not automatically generate amplification maps. In order to derive this, the adopted formula from Lee (*Lee et al.*, 2009b) was applied. PGA value for the model without topography from the model with topography was subtracted, then divided by PGA value from DEM without topography, and multiplied by 100 to get a percentage. This processed was done using ArcGIS 9.3 raster analysis.

- Synthetic seismogram records

  The synthetic seismogram records for each simulation are plotted in graphs. Followed this, the result was compared to analyze the impact of topography, mesh resolution and DEM resolution.

3.6. Analysis

In order to observe the amplification factor, we located a profile in the amplification maps as we can see in Figure 3.8 and plotted the amplification factor on a graph. The model output was analyzed in term of DEMs and mesh resolutions. Followed this, the amplification factor of model output were compared and analyzed in the context of DEMs and mesh resolutions.

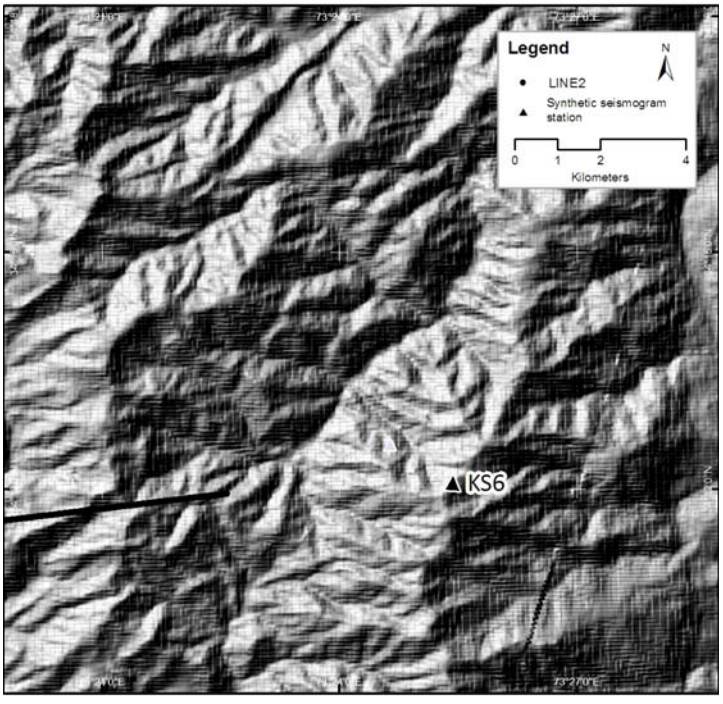

Figure 3.8 Map of synthetic seismogram and profile location

3.7. Haiti seismic amplification model

During the research, a 7 magnitude earthquake occurred in Haiti on 12 January 2010. The epicenter located in 18.45 north and 75.533 W with 13 km depth. Although this scenario is not included in our proposed method, the seismic amplification modelling was spontaneously applied based on this earthquake source characteristic using ASTER with coarse mesh (24x24) to investigate the performance of the model in rapid time.

4. Results

The results are presented within this chapter and further subdivided into two sub-chapters . The first sub-chapter is about accuracy assessment where the fieldwork data and its statistical data were presented. Results from seismic amplification modelling were shown along with its presentation in the second sub-chapters.

4.1. Results from accuracy accuracy assessment

To perform an accuracy assessment of DEMs, ground truth points were collected in the field. The elevation measurements were plotted in conjunction with DEM values, and the comparison was statistically analyze using RMSE and R^2 calculation. For further analysis on slope based, the data were divided into two groups based on slope degree. Slope angles of more than 10 degrees are categorized as sloping terrain whilst slope angles less than 10 degrees are categorized as flat surfaces. Following this, RMSE and R^2 were computed for each group.

4.1.1. Over-all statistical analysis

GCPs were collected from the field work and post-processed with differential correction. 4647 elevation points were measured where 32% are located in the sloping area with 10 degrees slope and the rest are from an area with less than 10 degrees or considerably flat surfaces. All the profiles taken are shown by the maps in Figure 3.4 (see Chapter 3.3.3)

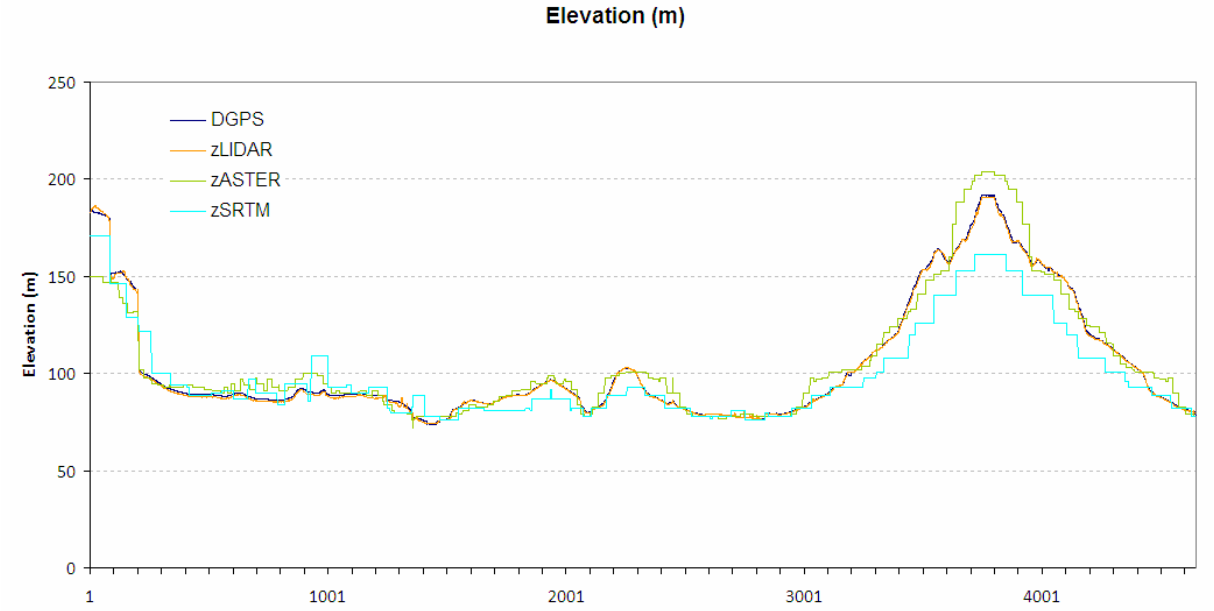

Figure 4.1 Plot of elevation from DGPS measurement, LiDAR, ASTER and SRTM. LiDAR overlapped precisely with DGPS data, ASTER and SRTM shows disparity with DGPS measurement.

GCPs measurement from DGPS were plotted in conjunction with ASTER, SRTM and LiDAR DEMs value extracted from the same points, as shown in Figure 4.1. The profile shows that

data from DGPS measurement and LiDAR are almost equivalent, whilst there is a discrepancy between DGPS measurement and both ASTER or SRTM. The differences were found larger on hills and slopes. Generally, SRTM tends to under-estimate while ASTER tends to over-estimate the hill elevation, particularly in elevated hills and steep slopes.

Based on RMSE calculations, from 4647 points as shown in Table 4.1, SRTM inherited the higher error than ASTER and LiDAR compromise the lowest error. These RMSE numbers are reflected in Figure 4.2, where DGPS and LiDAR data coincides almost perfectly along the regression line within the scatter plot, while ASTER and SRTM shows a disparity particularly in the area with high elevation. The calculated R^2 number shows that LiDAR has the best fit to model real terrain data.

Table 4.1 RMSE and R^2 calculation of over-all accuracy assessment

	LIDAR	**ASTER**	**SRTM**
COUNT	4647	4647	4647
RMSE (m)	**0.848**	**8.377**	**11.200**
R^2	0.9995	0.9336	0.9332

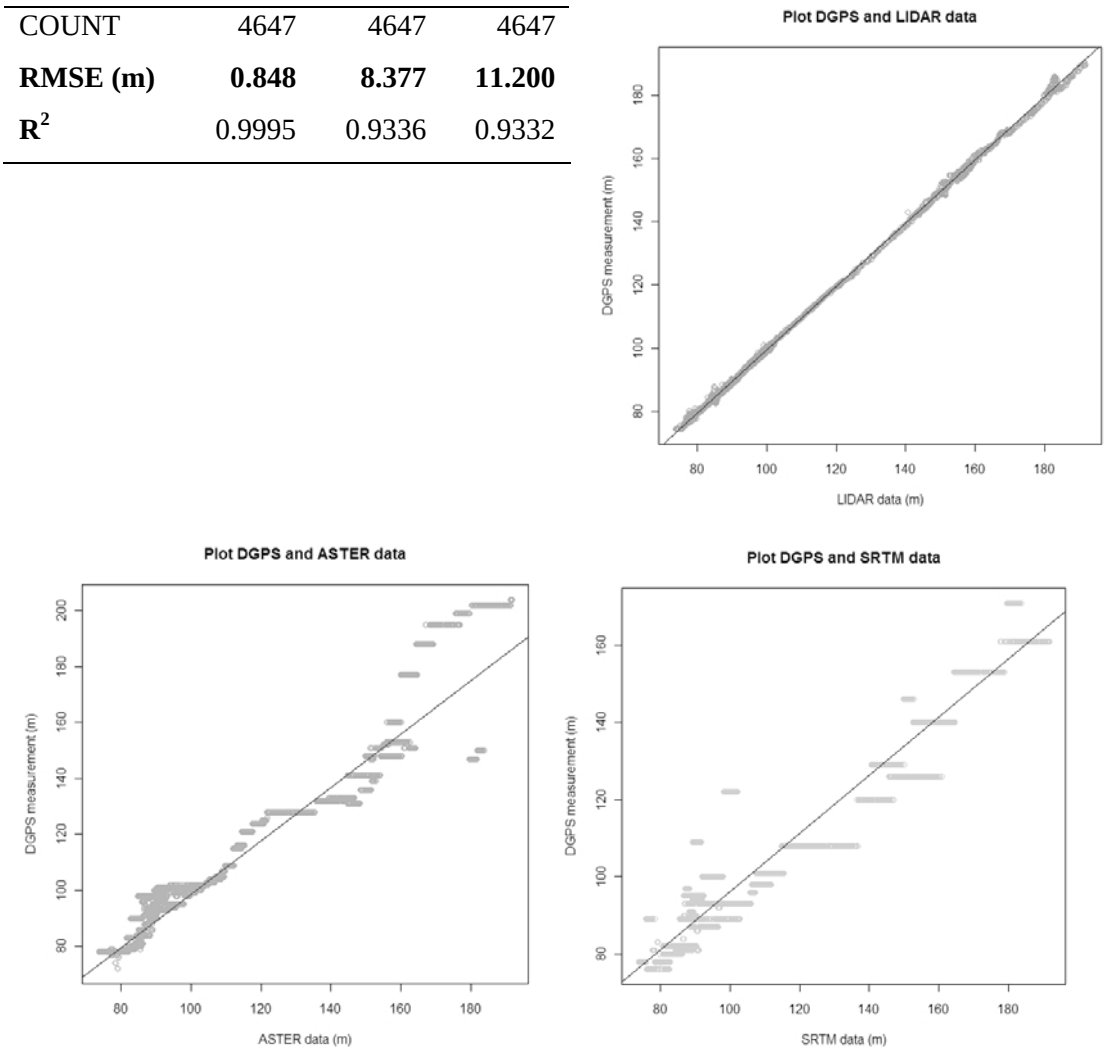

Figure 4.2 Scatter plot of DGPS and DEMs data, up: LiDAR, lower left: ASTER, lower right SRTM. LiDAR data overlapped precisely with DGPS measurement along the regression line while ASTER and SRTM shows disparity.

4.1.2. Slope based statistical analysis

The RMSE calculated from 3040 points on flat surface (Table 4.2.a) shows that all DEM measurements on the flat surface inherited less error than DEM estimates in sloping terrain (Table 4.2.b). Still, LiDAR is the most accurate DEM compared to ASTER and DEM and based on R^2 calculations, real world data is best predicted by LiDAR, both on flat surfaces or sloping terrain.

In the case of ASTER and SRTM, ASTER is more accurate, both on flat surfaces and sloping terrain. Table 4.2.a shows ASTER also performs better prediction of real world topography on flat surface, R^2 calculation from shows that SRTM estimates the earth's surface better on the slope and hills.

Table 4.2 RMSE and R2 calculation for accuracy assessment in a) sloping terrain and, b) flat surface

a)	LIDAR	ASTER	SRTM
COUNT	3040	3040	3040
RMSE	0.711	5.334	7.233
R^2	0.9991	0.9081	0.8239

b)	LIDAR	ASTER	SRTM
COUNT	1607	1607	1607
RMSE	1.059	12.211	16.241
R^2	0.9994	0.9071	0.9399

4.2. Seismic amplification modelling result

In this sub chapter, the result of seismic amplification modelling including the interpretation is shown. Shear wave velocity, PGA and amplification factor distribution are presented together with the interpretation and observation. Graphs from amplification along profiles and synthetic seismogram records are also shown. Additionally, we present PGA amplification from seismic amplification modelling of Haiti in the end of this chapter.

4.2.1. Shear wave velocity distribution

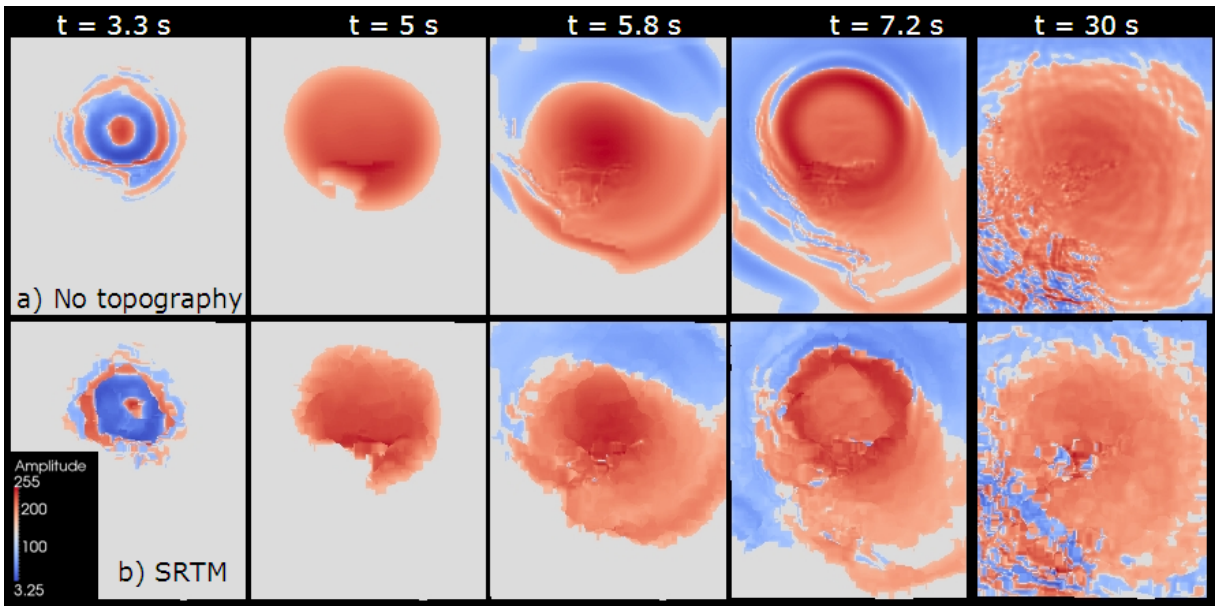

Figure 4.3 Snapshots of the SRTM fine mesh seismic wave propagation shown by shear wave velocity (cm/s^2): a) without topography, b) with topography. Red colours indicate positive value and blue colour indicates negative values. The wave patterns are dispersed by topography.

The series of amplitude maps as seen in Figure 4.3 illustrates how the seismic wave propagates from the point source and capture the time simulation of 3.3 s, 5 s, 5.8, 7.2 s and t = 30 seconds. Red colour indicated high velocity and blue colour indicated low velocity, thus the high contrasts of deep red and deep blue show a large top to peak amplitude of seismic waves.

At t = 3.3s the P body waves dominated the area with the high velocity near the epicentre. Notice that the circular pattern of the waves are scattered by the topography, resulting in complicated patterns of the wave propagation in local site. Surface waves reached the earth's surface and start spreading at t = 5.5 s with high amplitude and highest velocity concentrated in the spot near the epicenter. The round and smooth patterns of surfaces dispersed and scattered by topography as shown by rough pattern at the border of surface wave patterns.

The wave propagation direction is started to exhibit at t = 5.8 s where the general pattern of both simulations show that waves spread from the diagonal fault line to north east and south west direction of the area. This pattern continued to show at t = 7.2 and t = 30 s. Notice that in t = 7.2 s the high velocity in the south west is not existing in simulation without topography, but after t = 30 s this site is still dominated by high contrast amplitude in simulation with SRTM incorporated.

4.2.2. Peak ground acceleration (PGA) distribution

PGA distribution from all fine mesh (64) SRTM simulation scenarios are displayed in Figure 4.4. with a hillshading of SRTM as background. From simulation without topography we can see the influence of focal mechanism of the earthquake source dominated the PGA distribution pattern whereas the high PGA were located in the north east and the south west of the study area.

This distribution pattern was also displayed by topography incorporated simulation with the additional impact of terrain attributes which created a more complex pattern locally. Notice that in the south west part of the study area, high acceleration value from simulation with no topography were divided into two parts in the SRTM and ASTER simulation, where high acceleration occurred in the left side of the hill slope. Based on the direction of the wave propagation and the direction of these slopes affected by the incoming seismic waves, reflection, refraction and complex wave patterns are created which results in high amplification on those very slopes. SRTM and ASTER simulation shows very similar PGA distribution patterns with small variation of PGA values locally.

4.2.3. Amplification maps

Amplification distribution is derived from the PGA distribution with the formula adopted from Lee (*Lee et al.*, 2009b). The final amplification maps of all scenarios are shown by Figure 4.5. Here we can see the computed amplification maps from SRTM simulation, both for coarse (16) and fine (64) mesh, overlaid with hill shade map derived from SRTM DEM. The amplification value was quantified as percentage and displayed as a gradual red to blue colour with pale yellow in between. Amplification was denoted with positive value and de-amplification was denoted with negative value.

Generally, the distribution pattern of amplification is higher in the north part of the area. The amplification distribution pattern does not always correlate with the topography attributes like terrain and ridges. The high frequency content along the fault caused a large amplification located in the diagonal axis of the area, especially in the central part (1). Here the amplification factor is very high although it is located in the valley.

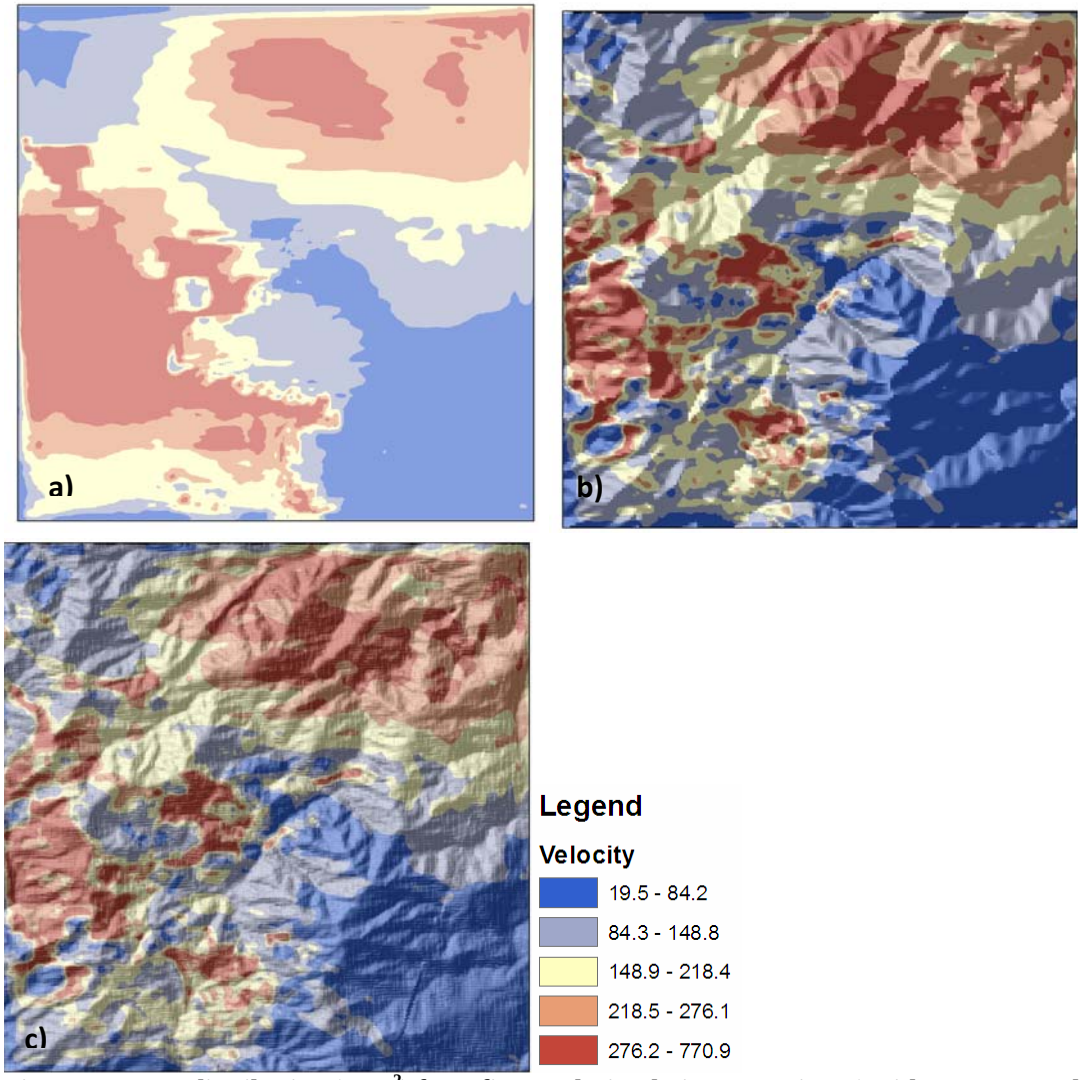

Figure 4.4 PGA distribution (cm/s^2) from fine mesh simulation scenarios: a) without topography, b) SRTM simulation overlaid with hillshade of SRTM, c) ASTER simulation overlaid with hillshade of ASTER.

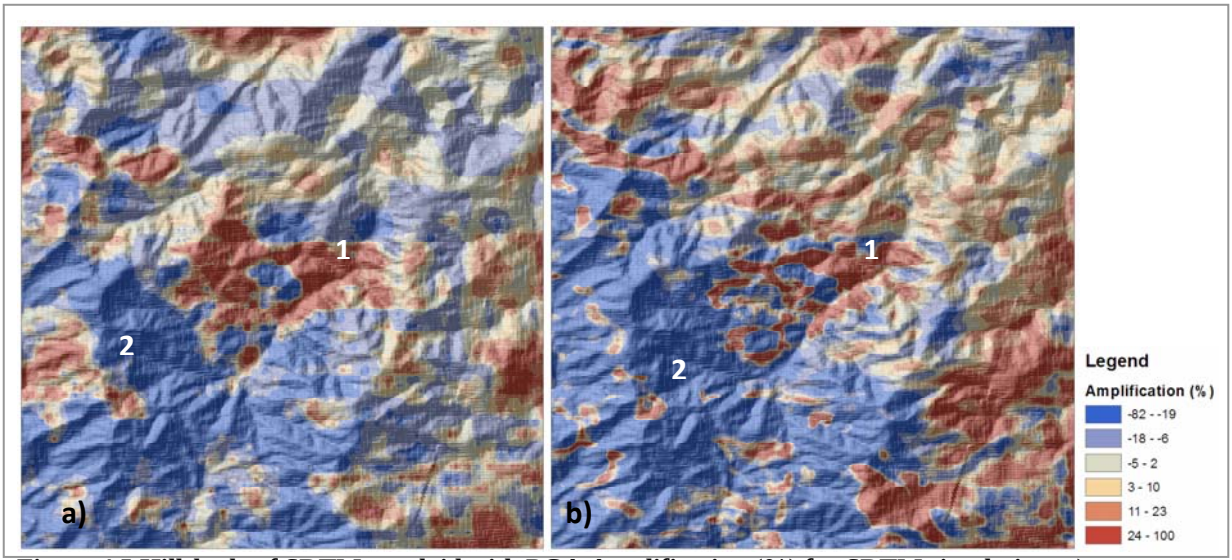

Figure 4.5 Hillshade of SRTM overlaid with PGA Amplification (%) for SRTM simulation, a) coarse mesh (16), b) fine mesh (64). Amplification are concentrated along the fault line, diagonally from north west to south east.

Simulation of coarse and fine mesh resulted in similar patterns for amplification distribution although fine mesh simulation results in a higher amplification factor and concentrated them in a smaller area. Coarse mesh simulation shows a large amplification occurred in the south west area, particularly on the western slope of the hills (2), while using a fine mesh simulation result shows the seismic wave is trapped in the peak of ridges, causing high amplification concentrated as spots. The inclined wave interacts with the slope angle, reflected and packed in the hill top (see Chapter 2.1.2, Figure 2.2), accordingly the trapped wave in the hill top results high amplification. Fine mesh simulation constructed with finer details of terrain, and consequently finer mesh performs a more realistic topography and incorporates more details of the hills. The complete amplification distribution is shown in Appendix D.

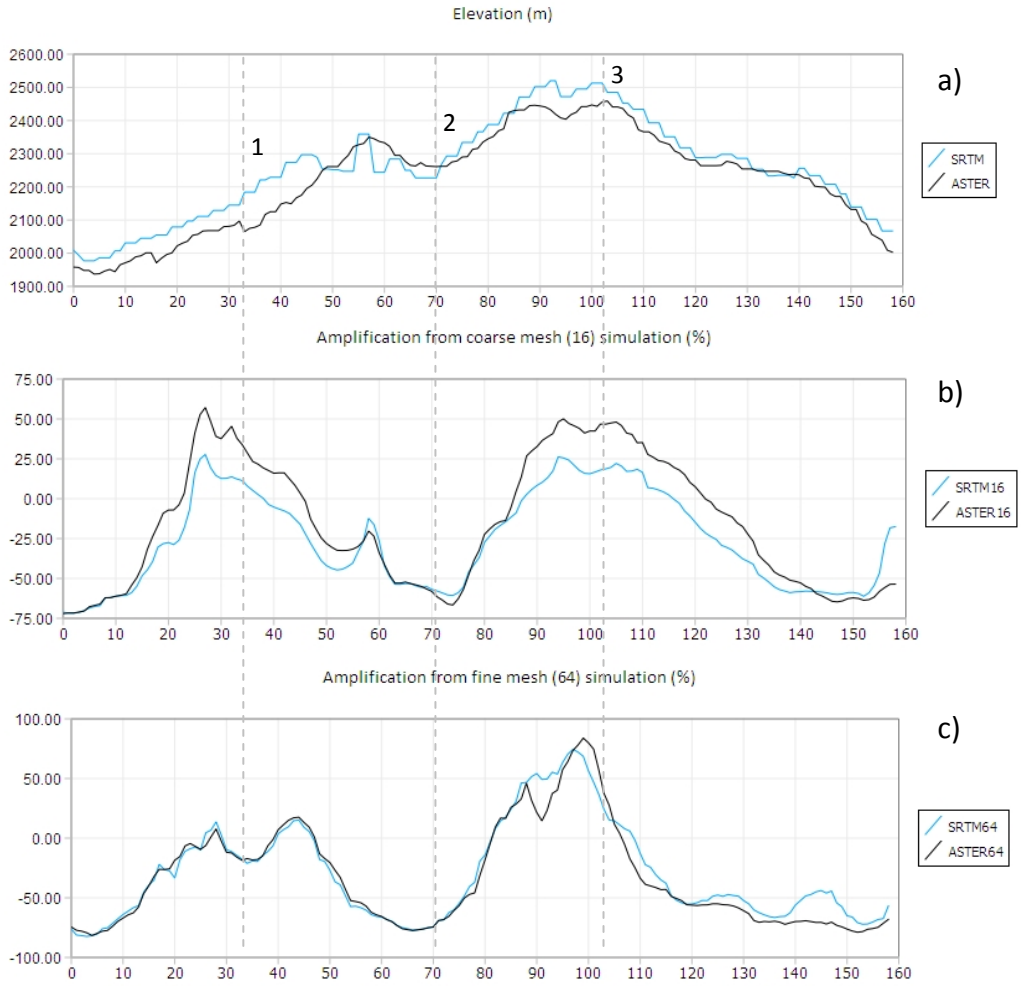

Figure 4.6 Profile of amplification from a) coarse mesh (16) simulation, and b) fine mesh (64)

4.2.4. PGA profile graph

We compare the amplification from coarse and fine mesh of SRTM simulation in Figure 4.5.b and 4.5.c, complemented by elevation profile. PGA amplification is varied from up to 60% in the coarse mesh simulation result while fine mesh resolution shows higher PGA amplification in variation of 75%. Fine mesh shows similar trend of simulation result between ASTER and SRTM and only varies very small while there is a disparity of PGA amplification between simulation using SRTM and

ASTER in the coarse mesh simulation. The disparity up to 25% can be found particularly at the ridges (3) while in the valley (2) there is no disparity of de-amplification.

Both coarse mesh and fine mesh shows similar trends of amplification factor along the profile except at (1) where coarse mesh simulation result shows high amplification on the slope. In the right part of (3) hill, coarse mesh also shows more gentle amplification curves than the fine mesh resolution results. The profile of amplification shows how terrain DEM attributes interact with seismic waves and impact on the amplification value.

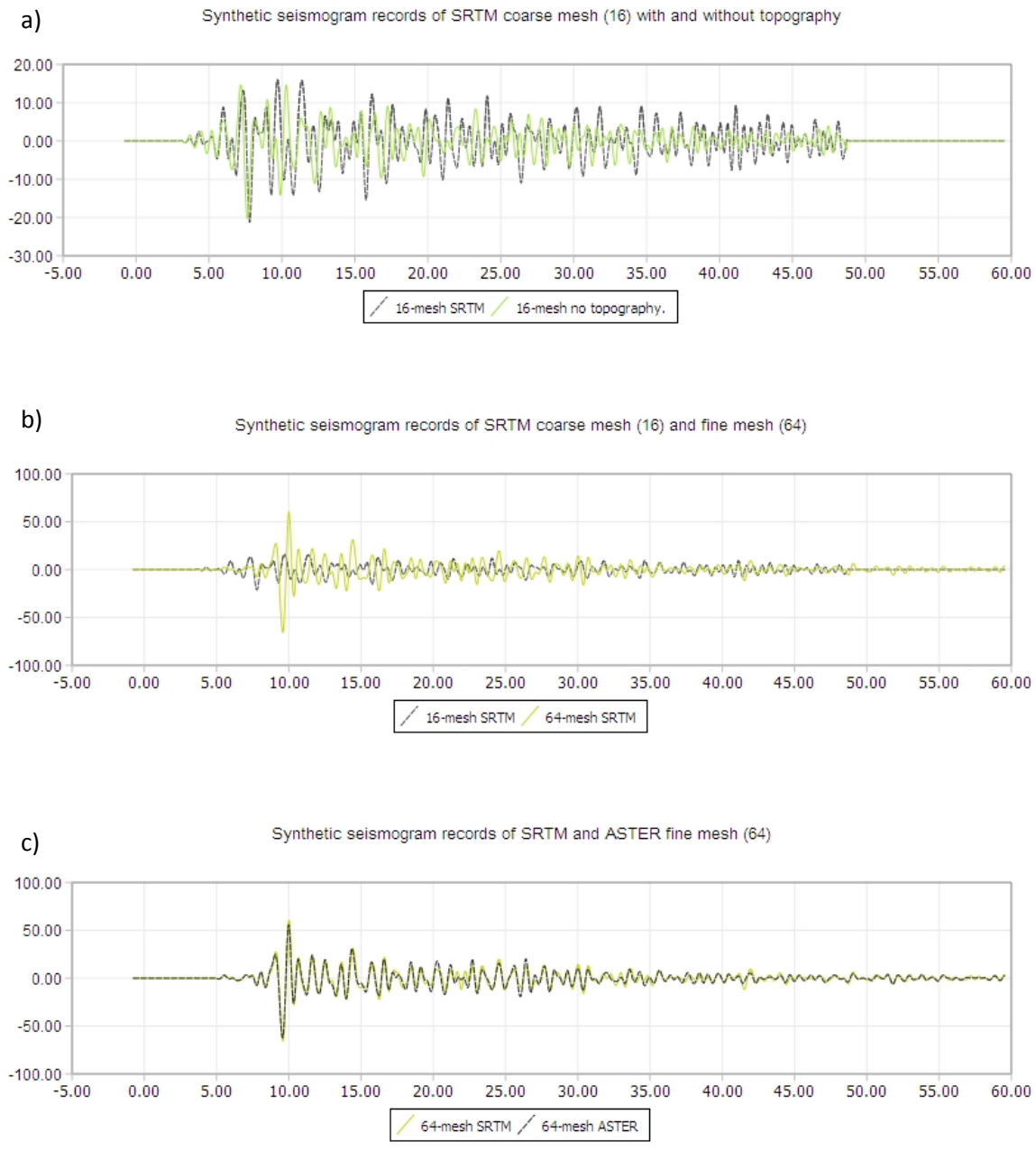

Figure 4.7 Synthetic seismogram records from station KS6 where we compare velocity result from: a) SRTM simulation of coarse mesh (16) with no topography and with topography, b), simulation of SRTM with coarse mesh (16) and fine mesh (64), and c) simulation with SRTM and ASTER fine mesh (64). The x axis indicates the time of the recordings and y axis shows velocity value in cm/s^2

4.2.5. Synthetic seismogram records

The 60 minutes synthetic seismogram records of station KS6 are shown by Figure 3.8. Station KS6 is located on the surface crest where we expect to find amplifications. Here we compared the seismogram records between, a) simulation with no topography and with topography, b) simulation with coarse mesh and fine mesh c) fine mesh simulation with SRTM and ASTER. The synthetic seismogram records show that topography amplified the seismic wave and it caused a longer duration of ground shaking during the 60 minutes of recording. From a comparison of synthetic seismogram records of different mesh resolution, we can see the shear wave velocity was amplified in factor of 4 which and consequently resulting a higher amplification at the arrival of surface waves. There are no significant differences of synthetic seismogram records between simulation using SRTM or ASTER.

4.2.6. Haiti seismic amplification distribution

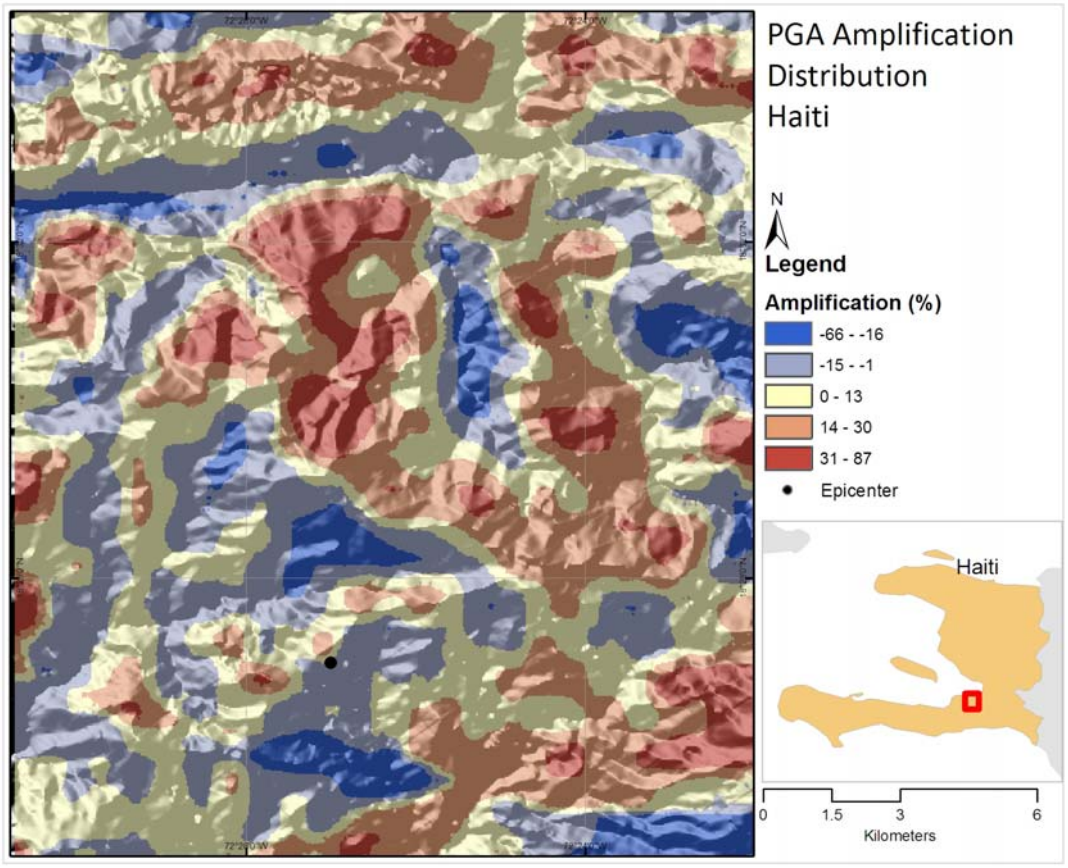

Figure 4.8 Map of Haiti amplification (5) distribution. Large amplification almost on all ridges.

Map of Haiti amplification distribution is shown by Figure 4.8. In Haiti, large PGA amplification clearly can be seen in ridges and peak of hills. In the upper part of the study area there is a fault line and seismic wave is largely attenuated in here. Highest amplification occurs in the highest elevation of hills within the central part of the study area.

5. Discussion and Conclusions

5.1. Discussions

5.1.1. Topographic impact on regional seismic amplification modelling

Based on the results of this research, there was a clear evidence of topography on variation of seismic response. The topographic impact can be observed from wave propagation patterns as shown by simulation outputs (see Chapter 4.2.1, Figure 4.3) where variety of terrain attributes dispersed and scattered the wave propagation into more complicated patterns. Topographic effect on seismic response was also shown by synthetic seismogram records (see Chapter 4.2.5, Figure 4.7) where the amplitude of seismic wave was amplified, particularly at the beginning of ground motion. The records also proven that topography caused longer duration of ground shaking. In addition, the topographic effect is also noticeable from the distribution pattern on PGA maps (see Chapter 4.2.3, Figure 4.5).

General findings from amplification maps show that high amplifications were found near the earthquake's epicentre and north and east part of Kashmir study area, separated by a diagonal line from north-west to southeast following the line of surface rupture. This result was confirmed by the intensity distribution pattern based on the near-field survey immediately after the earthquake, , which tend to be concentrated along the rupture line whereas the large ground shaking intensity of Kashmir earthquake 2005 did not follow a radial pattern (*Ali et al.*, 2009).

Related to the topographic impact on amplification distribution, amplification can be found on ridges. This condition was found by Lee (2009) on Yamingshan earthquake where there was a large amplification on a Chinese university location which happened to be on a flat surface (*Lee et al.*, 2009a). Although this finding was not prominent in his study, it was revealed that in some cases ridges does not always amplify the seismic response.

In the case of the Kashmir earthquake, regional seismic amplification is highly influenced by the source frequency content which might be considered the dominant factor that caused a large amplification in the valley near the epicentre (see Chapter 4.2.3, Figure 4.5). Northern part of the model area is also a relatively flat surface hence the PGA was not largely amplified although this area was dominated by large PGA (see Chapter 4.2.2, Figure 4.5) due to the focal mechanism of Kashmir earthquake source characteristic. However, amplification can be observed in some ridges and the values ±75%, larger than the findings of 50% from Lee (2009b) and Lee (2009a).

The effect of slope on Kashmir seismic amplification modelling can be spotted in some location (see Chapter 4.2.3, Figure 4.5) where slopes on the hill (2) impacted PGA distribution by concentrating them on the right slope of the hill. The effect of slope although have proven to be very prominent (*Ashford et al.*, 1997) but it is not always true in all cases. Slope might have increased amplification but the effect of directivity and depth of the event in respect to slope location and slope aspect, have to be taken account (*Lee et al.*, 2009b).

The regional seismic amplification modelling of Kashmir is limited by mesh design factor. In SEM, mesh design is a significant factor to perform accurate calculation (*Chaljub et al.*, 2007; *Komatitsch and Tromp*, 1999; *Lee et al.*, 2009b). Several buffer layers are usually assigned near the

mesh surface to dampen mesh distortions of undulating topography particularly on steep terrain (*Lee et al.*, 2009b). On a local scale seismic amplification modelling incorporating high resolution DEM, Lee (2009a) include three buffer layers in the designed mesh, and similarly Lee (2009b) use the same number of layers for modelling seismic amplification in a large scale area. Due to the limitation of computation capability, Kashmir topographic amplification model was designed with incorporating two buffer layers in a mesh. This mesh design might be a significant factor to simulate topographic amplification in a largely varying topography like Kashmir where the distortion can possibly occur on steep slope and pointed hills.

Another restraint of mesh design of Kashmir simulation is the mesh resolution. Kashmir regional seismic amplification modelling was designed with very coarse mesh of 16 grid and finer mesh of 64 grid due to the computational capacity. The finer mesh of 64 does not apply the same grid resolution with the actual resolution of DEMs. Therefore, the preserved topography on top of the mesh was resampled according to the mesh resolution. Additionally, the result from the Kashmir simulation tested with various mesh resolutions has proven that finer mesh produced a more consistent output.

Seismic amplification model's computational code has been verified for simulating wave propagation incorporated realistic earthquake characteristic including the topography effect (*Komatitsch and Tromp*, 2002a). On the other hand, validation for Kashmir seismic amplification in a concern of cross-checking with ground truth of ground shaking amplification data was not accomplished due to the lack of real seismogram records of 2005 Kashmir earthquake. However, this validation is possible to achieve in a future works if ground shaking data is available.

5.1.2. DEM resolution and accuracy issue in regional seismic amplification modelling

The LiDAR as high resolution DEM was proven to contain smallest error among the utilized DEMs and proven the best predictor for earth model. The ASTER which is a higher resolution DEM than SRTM consists of less inherent error, proven by the computed RMSE. In a case of sloping terrain, computed R^2 value shows that SRTM performs better prediction for earth true surface although its resolution is coarser than ASTER. Shafique (2008) also addressed that SRTM was proven to be more consistent to slope and aspect computations. This evidence is important to be noted before applying DEMs in the model in future works.

In the case of Kashmir regional seismic amplification modelling, the effects of ASTER and SRTM resolution were assessed to illustrate seismic responses on DEMs derived attributes. Based on the result of regional scale simulation, DEMs resolution has no significant influence on the seismic amplification modelling simulation. The similar trend can be observed from result of fine mesh resolution where the amplification profile from both simulation of ASTER and SRTM shows similar tendencies (see Chapter 4, Figure 4.6). This findings agree with that of Shafique's (2009) conclusion in his research of assessing topographic parameters from ASTER and SRTM to predict seismic amplification using Geospatial tools.

On the contrary, based upon a local scale seismic amplification modelling, Lee (2009a) , recommended the utilization of fine resolution DEMs. In the case of local scale amplification modelling, DEMs play an important role since the model required small details of terrain attribute to indicate the amplification on the local site. The simulation on a local scale model of 4 x 3 km (*Lee et al.*) was performed with LiDAR with 2 m resolution and 40 m DEM, while in Kashmir model we analyzed the influences of SRTM with 90 m resolution versus ASTER with 30 m resolution on regional scale seismic amplification modelling. Comparatively, the ratio between DEMs resolution's

of 90 and 30 m is lower then 40 m and 2 m. Therefore, the resolution plays important role in local scale while it is not a significant factor for regional topographic seismic amplification modelling.

Still on a scale based issue, topographic amplification modelling on a regional scale using medium resolution DEMs appeal to perform better for a big earthquake with more than 7 magnitude, for example a case study of 2005 Kashmir and 2010 Haiti. This is due to the fact that big earthquakes have higher frequency contents and widespread destruction. Source frequency content is sensitive for topographic amplification, thus the small details of fine resolution DEMs will exaggerate amplification. The extent of big earthquake also complies with regional scale of seismic amplification modelling, where DEM resolution tends to show more general pattern of terrain attribute for wider areas. Additionally, using fine resolution DEMs on regional scale seismic amplification can add a lot of cost to the computational time of simulation.

5.1.3. Haiti regional seismic amplification modelling

Based on the rapid seismic amplification simulation with Haiti's earthquake source characteristics, generally the PGA amplification show the occurrence of amplification in the ridges and de-amplification was appeared in the valley. Amplification also was found in the slopes facing the directivity of seismic wave propagation. The amplification distribution pattern correlated to the topography within the Haiti study area.

Although this Haiti simulation was not included in the research objective, rapid work for Haiti simulation shows that the regional seismic amplification modelling with medium resolution DEMs can be simultaneously applied to model the ground shaking with more realistic earthquake source characteristics and incorporating topographic effects. This finding can be benefit for near real-time regional modelling of seismic amplification, particularly on emergency phase of earthquake disaster.

5.2. Conclusions

The impact of topography of seismic response can be evaluated realistically taking into account the seismic source, medium and topography as site effect in 3D environment. The three dimensional model incorporating DEM derived from ASTER and SRTM DEMs, is proven to be sufficient to model the seismic wave propagation at a regional scale.

Topographic impact of amplified seismic response observed during 2005 Kashmir earthquake, although the general pattern of amplification is dispersed and dominated by the fault rupture. Higher amplifications are found in the north and east part of the study area separated by a diagonal line from north west to south east following the line of surface rupture.

The amplification factor in Kashmir seismic amplification modelling varies by ± 75% and the difference in amplification between a valley and a ridge can be as high as a factor of 2. In spite of the demonstrated topographic impact on seismic response in Kashmir simulation, regional topographic seismic amplification modelling of Kashmir is limited by computational capabilities causing a coarse mesh design and inability to include more than one buffer layers.

There is not a significant difference between the various resolution and accuracy of applied DEM on seismic amplification modelling result. However, concerning the issue of consistency, SRTM as the more consistent DEM shows reliable results from diverse mesh structure of the computation.

In addition, regional topographic seismic amplification can be applied promptly and demonstrate the ground shaking distribution with more realistic earthquake characteristic, taking into account topography as site effects.

5.3. Recommendations

As topography have proven to have significant effect to seismic response, it is important to include this effect in the future work of more realistic model of seismic propagation and ground shaking prediction. The mesh design should be considered carefully, especially in a large varying topography with steep slopes and pointed hills.

Due to the lack of ground shaking records from the seismogram network in the study area, the validation of regional seismic amplification of Kashmir earthquake was not accomplished. The available ground shaking records should be taken into account for validating the simulation in a future works.

Kashmir area is a rough terrain which has not only large varying topography, but also very diverse geologic structures. Furthermore, the deep valley of Kashmir is dominated by alluvial flood plains with thick soil cover. The effect of soil and geology on ground shaking have proven to be prominent and dominated in specific sites. Therefore, the soil and geology should be incorporated to expand the regional ground shaking amplification modelling with realistic earthquake characteristics.

References

Aguilar, F.J., Aguilar, M.A. and AgÃ¼era, F., 2007. *Accuracy assessment of digital elevation models using a non-parametric approach*. International Journal of Geographical Information Science, 21(6): 667-686.

Alexander, D., 1993. *Natural Disaster*. USL Press, London.

Ali, Z. et al., 2009. *Muzaffarabad, earthquake of 8 October 2005: surface faulting, environmental effects and macroseismic intensity*. In: K. Reicherter, A.M. Michetti and P.G. Silve (Editors), Palaeoseismology: Historical and prehistorical records of earthquake ground effects for seismic hazard assessment. Geological Society of London, London, pp. 332.

Allen, R.M. and Gerald, S., 2007. *Earthquake Hazard Mitigation: New Directions and Opportunities*, Treatise on Geophysics. Elsevier, Amsterdam, pp. 607-647.

Anderson, D.L. and Hart, R.S., 1978. *Attenuation models of the earth*. Physics of the Earth and Planetary Interiors, 16(4): 289-306.

Ashford, S.A. and Sitar, N., 1997. *Analysis of topographic amplification of inclined shear waves in a steep coastal bluff*. Bulletin of the Seismological Society of America, 87(3): 692-700.

Ashford, S.A., Sitar, N., Lysmer, J. and Deng, N., 1997. *Topographic effects on the seismic response of steep slopes*. Bulletin of the Seismological Society of America, 87(3): 701-709.

ASPRS, A.S.f.P.a.R.S., 2004. *Vertical Accuracy Reporting for Lidar Data*, Maryland, USA, pp. 20.

ASTER GDEM, V.T., 2009. *ASTER Global DEM Validation - Summary Report*, METI/ERSDAC, NASA/LPDAAC, and USGS/EROS.

Athanasopoulos, G.A., Pelekis, P.C. and Leonidou, E.A., 1999. *Effects of surface topography on seismic ground response in the Egion (Greece) 15 June 1995 earthquake*. Soil Dynamics and Earthquake Engineering, 18(2): 135-149.

Boore, D.M., 1972. *A note on the effect of simple topography on seismic SH waves*. Bulletin of the Seismological Society of America, 62(1): 275-284.

Boore, D.M., 1973. *The effect of simple topography on seismic waves: Implications for the accelerations recorded at Pacoima Dam, San Fernando Valley, California*. Bulletin of the Seismological Society of America, 63(5): 1603-1609.

Bouchon, M., 1973. *Effect of topography on surface motion*. Bulletin of the Seismological Society of America, 63(2): 615-632.

Bouckovalas, G.D. and Papadimitriou, A.G., 2005. *Numerical evaluation of slope topography effects on seismic ground motion*. Soil Dynamics and Earthquake Engineering, 25(7-10): 547-558.

Casarotti, E. et al., 2008. *CUBIT and Seismic Wave Propagation Based Upon the Spectral-Element Method: An Advanced Unstructured Mesher for Complex 3D Geological Media*, Proceedings of the 16th International Meshing Roundtable, pp. 579-597.

Castrignanò, A.B., G; Comolli, R; Ballabio, C, 2006. *Accuracy assessment of digital elevation model using stochastic simulation*. Dipartimento Di Scienze Dell Ambiente e Del Territorio.

Celebi, M., 1987. *Topographical and geological amplifications determined from strong-motion and aftershock records of the 3 March 1985 Chile earthquake*. Bulletin of the Seismological Society of America, 77(4): 1147-1167.

Chaljub, E. et al., 2007. *Spectral-element analysis in seismology*, Advances in Geophysics. Elsevier, pp. 365-419.

Chavez-Garcia, F.J., Sanchez, L.R. and Hatzfeld, D., 1996. *Topographic site effects and HVSR. A comparison between observations and theory*. Bulletin of the Seismological Society of America, 86(5): 1559-1573.

CMT, C.P., 2006. *Global CMT Web Page*.http://www.globalcmt.org/. 20 January 2010: 20 January 2010

Davis, L.L. and West, L.R., 1973. *Observed effects of topography on ground motion*. Bulletin of the Seismological Society of America, 63(1): 283-298.

Delavaud, E., Vilotte, J.P., Festa, G. and Cupilard, P., 2006. *3D Spectral Element Method Simulations of the Seismic Response of Caracas (Venezuela) Basin*, Third International Symposium on the Effects of Surface Geology on Seismic Motion, Grenoble, France, pp. 8.

E. Rodríguez, C.S.M., J.E. Belz, E.C. Chapin, and J.M. Martin, W.D., S. Hensley, 2003. *An Assessment of the SRTM Topographic Products*, Jet Propulsion Laboratory, Pasadena, California.

Erdik, M. and Durukal, E., 2004. *Strong Ground Motion*, Recent Advances in Earthquake Geotechnical Engineering and Microzonation, pp. 67-100.

FGDC, F.G.D.C., 1998. *Geospatial Positioning Accuracy Standards*, Part 3: National Standard for Spatial Data Accuracy. Federal Geographic Data Committee Secretariat, Virginia, pp. 28.

Frankel, A. and Vidale, J., 1992. *A three-dimensional simulation of seismic waves in the Santa Clara Valley, California, from a Loma Prieta aftershock.* Bulletin of the Seismological Society of America, 82(5): 2045-2074.

Geli, L., Bard, P.-Y. and Jullien, B., 1988. *The effect of topography on earthquake ground motion: A review and new results*. Bulletin of the Seismological Society of America, 78(1): 42-63.

Geodynamics, C.I.f., 2009. *SPECFEM3D*.http://www.geodynamics.org/cig/software/packages/seismo/specfem3d/. 10 August 2009: 10 August 2009

Gorokhovich, Y. and Voustianiouk, A., 2006. *Accuracy assessment of the processed SRTM-based elevation data by CGIAR using field data from USA and Thailand and its relation to the terrain characteristics*. Remote Sensing of Environment, 104(4): 409-415.

Hestholm, S., 1999. *Three-dimensional finite difference viscoelastic wave modelling including surface topography*. Geophysical Journal International, 139(3): 852-878.

Hestholm, S. et al., 2006. *Effects of free-surface topography on moving-seismic-source modeling*. Geophysics, 71(6): T159-T166.

Jing, L., 2003. *A review of techniques, advances and outstanding issues in numerical modelling for rock mechanics and rock engineering*. International Journal of Rock Mechanics and Mining Sciences, 40(3): 283-353.

Komatitsch, D. et al., 2004. *Simulations of Ground Motion in the Los Angeles Basin Based upon the Spectral-Element Method*. Bulletin of the Seismological Society of America, 94(1): 187-206.

Komatitsch, D., Ritsema, J. and Tromp, J., 2002. *The Spectral-Element Method, Beowulf Computing, and Global Seismology*. Science, 298(5599): 1737-1742.

Komatitsch, D. and Tromp, J., 1999. *Introduction to the spectral element method for three-dimensional seismic wave propagation*. Geophysical Journal International, 139(3): 806-822.

Komatitsch, D. and Tromp, J., 2002a. *Spectral-element simulations of global seismic wave propagation - I. Validation*. Geophysical Journal International, 149(2): 390-412.

Komatitsch, D. and Tromp, J., 2002b. *Spectral-element simulations of global seismic wave propagation - II. Three-dimensional models, oceans, rotation and self-gravitation*. Geophysical Journal International, 150(1): 303-318.

Komatitsch, D. and Vilotte, J.-P., 1998. *The spectral element method: An efficient tool to simulate the seismic response of 2D and 3D geological structures*. Bulletin of the Seismological Society of America, 88(2): 368-392.

Lay, T. and Wallace, T.C., 1995. *Modern Global Seismology*. Academic Press, 521 pp.

Lee, S.-J., Chan, Y.-C., Komatitsch, D., Huang, B.-S. and Tromp, J., 2009a. *Effects of Realistic Surface Topography on Seismic Ground Motion in the Yangminshan Region of Taiwan Based Upon the Spectral-Element Method and LiDAR DTM*. Bulletin of the Seismological Society of America, 99(2A): 681-693.

Lee, S.J. et al., 2008. *Three-dimensional simulations of seismic-wave propagation in the Taipei basin with realistic topography based upon the spectral-element method.* Bulletin of the Seismological Society of America, 98(1): 253-264.

Lee, S.J., Komatitsch, D., Huang, B.S. and Tromp, J., 2009b. *Effects of Topography on Seismic-Wave Propagation: An Example from Northern Taiwan*. Bulletin of the Seismological Society of America, 99(1): 314-325.

Leica Geosystems, A., 2004. *GPS1200 - User Manual version 1.1*, Switzerland, pp. 142.

Li, Z., 1988. *ON THE MEASURE OF DIGITAL TERRAIN MODEL ACCURACY*. The Photogrammetric Record, 12(72): 873-877.

Li, Z., Zu, Q. and Gold, C., 2005. *Digital Terrain Modelling*. CRC Press.
Liu, X., Zhang, Z., Peterson, J. and Chandra, S., 2007. *The effect of LiDAR data density on DEM Accuracy*. In: L. Oxley and D. Kulasiri (Editors), MODSIM07 International Congress on Modelling and Simulation. Modelling and Simulation Society of Australia and New Zealand Inc., Christchurch, New Zealand, pp. 1363-1369.
Lowrie, W., 2007. *Fundamental of Geophysics.* Cambridge University Press, New York.
Lunetta, R.S. et al., 1991. *Remote Sensing and Geographic Information System Data Integration: Error Sources and Research Issues*. Photogrammetric Engineering and Remote Sensing (PE&RS): 11.
Ma, S., Archuleta, R.J. and Page, M.T., 2007. *Effects of Large-Scale Surface Topography on Ground Motions, as Demonstrated by a Study of the San Gabriel Mountains, Los Angeles, California*. Bulletin of the Seismological Society of America, 97(6): 2066-2079.
Mockton, C.G., 1994. *An investigation into the spatial structure of error in digital elevation data,* Innovations in GIS. Taylor & Francis, Bristol, pp. 201 - 207.
Murck, B.W., Skinner, B.J. and Porter, S.C., 1997. *Dangerous Earth - An Introduction to Geological Hazards*. John Miley & Sons, Inc., Canada, 300 pp.
Pitarka, A., 1999. *3D Elastic finite-difference modeling of seismic motion using staggered grids with nonuniform spacing*. Bulletin of the Seismological Society of America, 89(1): 54-68.
Pitarka, A., Irikura, K., Iwata, T. and Sekiguchi, H., 1998. *Three-dimensional simulation of the near-fault ground motion for the 1995 Hyogo-Ken Nanbu (Kobe), Japan, earthquake*. Bulletin of the Seismological Society of America, 88(2): 428-440.
Rabus, B., Eineder, M., Roth, A. and Bamler, R., 2003. *The shuttle radar topography mission--a new class of digital elevation models acquired by spaceborne radar*. ISPRS Journal of Photogrammetry and Remote Sensing, 57(4): 241-262.
Rao, N.P., Kumar, P., Kalpna, Tsukuda, T. and Ramesh, D.S., 2006. *The devastating Muzaffarabad earthquake of 8 October 2005: New insights into Himalayan seismicity and tectonics.* Gondwana Research, 9(4): 365-378.
Ripperger, J., Igel, H. and Wasserman, J., 2003. *Seismic wave simulation in the presence of real volcano topography*. Journal of Volcanology and Geothermal Research, 128(1-3): 31-44.
Shafique, M., 2008. *Predicting topographic aggravation of seismic ground shaking using geospatial tools : a case study of Kashmir earthquake, Pakistan.* MSc Thesis, ITC, Enschede, 112 pp.
Shafique, M., van der Meijde, M., Kerle, N. and van der Meer, F.D., 2009. *Impact of topographic parameters on seismic amplification applying geospatial tools*. In: Remote sensing for a changing Europe : proceedings of the 28th EARSeL symposium, 2-7 June 2008, Istanbul, Turkey / ed by. D. Maktav. Amsterdam : IOS Press, 2009. ISBN 978-1-58603-986-8-386. pp. 386-394.
Toutin, T., 2008. *ASTER DEMs for geomatic and geoscientific applications: a review*. Int. J. Remote Sens., 29(7): 1855-1875.
Towhata, I., 2008. *Geotechnical Earthquake Engineering*. Springer Verlag
697 pp.
UNISDR, 2006. *Disaster statistics 1991-2005*.http://www.unisdr.org/disaster-statistics/occurrence-type-disas.htm. 31 July 2009: 31 July 2009
USGS, 2009. *Historical Earthquake by country - Pakistan*.http://earthquake.usgs.gov/regional/world/historical_country.php#pakistan. 27 May 2009: 27 May 2009
USGS, 2010. *ShakeMaps*.http://earthquake.usgs.gov/eqcenter/shakemap/.

Appendix A

Table Showing Parameter File

parameters	options	SRTM				ASTER			
		No topography		With topography		No topography		With topography	
		Coarse mesh	Fine Mesh	Coarse mesh	Fine Mesh	Coarse mesh	Fine Mesh	Coarse mesh	Fine Mesh
type of simulation	forward	forward	forward	forward	forward	forward	forward	forward	forward
	adjoint								
	kernel								
mesh block information (in decimal degrees)	longitude (min, max)	73.432,73,793	73.432,73,793	73.432,73,793	73.432,73,793	73.321,73.906	73.321,73.906	73.321,73.906	73.321,73.906
(in decimal degrees)	latitude (min, max)	34.253,34.619	34.253,34.619	34.253,34.619	34.253,34.619	34.146,34.732	34.146,34.732	34.146,34.732	34.146,34.732
in km	block depth	40km	40km	40km	40km	40km	40km	40km	40km
	UTM projection zone	43	43	43	43	43	43	43	43
mesh grid	NEX_XI	**16**	**64**	**16**	**64**	**16**	**64**	**16**	**64**
	NEX_ETA	**16**	**64**	**16**	**64**	**16**	**64**	**16**	**64**
number of MPI processor used		1	1	1	1	1	1	1	1
fault model	SoCal	SoCal	SoCal	SoCal	SoCal	SoCal	SoCal	SoCal	SoCal
	Harvard_LA								
	Minchen anisotropy								
models parameter included	bathymetry	no	no	no	no	no	no	no	no
	topography	**no**	**no**	**yes**	**yes**	**no**	**no**	**yes**	**yes**
	attenuation	yes	yes	yes	yes	yes	yes	yes	yes
	olsen attenuation	yes	yes	yes	yes	yes	yes	yes	yes
absorbing boundary conditions	yes / no	yes	yes	yes	yes	yes	yes	yes	yes
record length of synthetic seismograms		60 minutes	60 minutes	60 minutes	60 minutes	60 minutes	60 minutes	60 minutes	60 minutes
recording parameter for output	movie surface	yes	yes	yes	yes	yes	yes	yes	yes
	movie volume	no	no	no	no	no	no	no	no
	time step per records	50	50	50	50	50	50	50	50
	shakemaps	yes	yes	yes	yes	yes	yes	yes	yes
	displacement	yes	yes	yes	yes	yes	yes	yes	yes
	movie hour	-	-	-	-	-	-	-	-
option for saving mesh files	yes / no	yes	yes	yes	yes	yes	yes	yes	yes
path to local databases		local database				local database			
interval between time step and maximum displacement		100	100	100	100	100	100	100	100
time step between seismograms recordings		200000	200000	200000	200000	200000	200000	200000	200000
option for recordings source time function	yes / no	yes	yes	yes	yes	yes	yes	yes	yes

Appendix B

CMT Solutions

(i) CMT Solution for Kashmir

```
PDE 2005 10  8  3 50 40.80  34.5400   73.5900  26.0 6.9 7.7 PAKISTAN
event name:     200510080350A
time shift:     10.6700
half duration:  15.0000
latitude:       34.3800
longitude:      73.4700
depth:          12.0000
Mrr:       2.610000e+27
Mtt:      -1.270000e+27
Mpp:      -1.330000e+27
Mrt:       1.430000e+27
Mrp:       3.640000e+26
Mtp:       1.260000e+27
```

(ii) CMT Solution for Haiti

```
PDE 2010  1 12 21 53  9.00  18.4500  -72.4500  10.0 7.0 7.0 HAITI
REGION
event name:     201001122153A
time shift:      0
half duration:   0
latitude:       18.4500
longitude:     -72.4500
depth:          12.0000
Mrr:       1.870000e+26
Mtt:      -4.050000e+26
Mpp:       2.180000e+26
Mrt:      -1.030000e+26
Mrp:      -1.290000e+26
Mtp:       2.830000e+26
```

Appendix C

SPECFEM3D-1.4.3 Manual Complementary

1. Input data

Convert the DEM

All the DEM preparation was performed in ArcGIS software. Notepad text editor is suitable for minor editing. The following are steps used to convert the DEM:

- **Make a square area from DEM (Create a region of interest from DEM)**
  Ensure all pixels have values.If this is not the case, pay attention to non-value pixels or missing pixels within the DEM. otherwise pay attention to non-value pixels
- **Flip the DEM raster files – The** *ArcToolbox* within ArcGIS is used. The *Data Management* application is selected and the function *Flip* is chosen.→ Data Management → Flip
  this is necessary since the model read the topography from left top corner as a 0,0 point and that's not the way latitude and longitude in the world start.
  This function is essential as the model reads the topography from the top left corner as a 0,0 point.
  NB: This is not the structure for latitude and longitude within the world setting.
- **Convert the DEM flip files into Points** – The *ArcToolbox* within ArcGIS is used. The *Conversion* application is selected and the function *From Raster to points* is chosen.→ Conversion → From Raster to points
  This produces point files with Pixel Values
- **Extract Values into .txt files**
  Export the table of point file into .txt file. Create a new field in the table. Copy the pixel value (grid code) with the field calculator. Convert this column to .txt files directly from the table., To ensure the outputs are correct, it is advisable to check the file with a text editor. Notepad was used to get rid of the unnecessary header information and saved as a .dat file. There, you have a topography file consisting of one column of elevation values. To avoid confusion of using this file in the script, it was renamed such as, topo_bathy_final.dat
- **Capture Raster properties**
  This is done by observing *Raster properties* in ArcGIS or converting the *raster into ASCII* file using ArcToolBox
  The idea is to obtain this information:
  1. Number of rows and columns
  2. Cell size
  3. Coordinates of top left corner of the DEM
  4. Coordinates of bottom right corner of DEM

Incorporating the DEM into the SPECFEM

- Place the topo_bathy_final.dat file in the model.

Place the file directly in SPECFEM3D-1.4.3 main folder in order to avoid long path of file name.

- Edit the constants.h file by typing: `nano constants.h`
  The part needs to be modified
  - Local path to Databases where the computation take places
    `LOCAL_PATH_Q = 'home/DATABASES_MPI_Q/'`
    Don't forget to make a specific folder called DATABASES_MPI_Q beside DATABASES_MPI
  - Topography file (although it is under warning: do not modify anything below)

  Line 230 -235

  `NX_TOPO_SOCAL = __,NY_TOPO_SOCAL = __` → number of rows and columns

  `ORIG_LAT_TOPO_SOCAL = __._d0` → top latitude in degrees

  `ORIG_LONG_TOPO_SOCAL = __._d0` → left longitude in degrees

  `DEGREES_PER_CELL_TOPO_SOCAL = __._d0 / 1000.0d0` → cell size in degrees

  `TOPO_FILE_SOCAL = '/home/topo_bathy_final.dat'` → path to topography file

  Save this new constants.h file

- **Edit Par_file** by typing: `nano DATA/Par_file`
  Adjust this Par_file according to the simulation design. The following is editable :

```
# coordinates of mesh block in latitude/longitude and depth in km
LATITUDE_MIN =
LATITUDE_MAX =
LONGITUDE_MIN =
LATITUDE_MAX =

NEX_XI =
NEX_ETA =
```

This defines the resolution of the model output. Must be 8 or 16 or 24 and so on.
The higher the number, the finer the model output resolution will be, but requires a longer computation time. From my experience 8 will run for approx. 10 minutes, while 32 will run the model for approx. 90minutes.

```
LOCAL_PATH =
```

Path for DATABASES_MPI folder

- Edit STATIONS file by typing `nano DATA/STATIONS`
  The model will only run with at least one synthetic seismogram station located in the area. We can add as many stations as we like by adding the coordinates and the name.

2. Running the software

Running the mesher

`./go_mesher`

```
make meshfem3D
./xmeshfem3D
```

Running the solver

In short, after providing the inputs and modifying the parameter file, type:

```
./go_solver
make specfem3D
./xspecfem3D
```

Note: After `./xmeshfem3D` process finished, a mesh is generated and this can be checked by generating DX file with command:

```
make combine_AVS_DX
./xcombine_AVS_DX
```

Choose an option either for surface topography or edge of the mesh then this process automatically generates DX_fullmesh.dx in folder OUTPUT_FILES. View this file using OpenDX.

3. Getting the output

Movie files

If the flag movie surface was set to .true. in the Par_file, moviedata?????? files are produced in OUTPUT_FILES for every time step according to the NSTEP_BETWEEN_FRAMES value.

- To **convert the data to readable image files**, type:

```
make create_movie_AVS_DX
./xcreate_movie_AVS_DX
```

Then **choose the options**

1 – for OpenDX format (DX__.dx), view these files with OpenDX

2 and 3 for AVS format

4 – for gmt format (gmt__.xyz), txt files with coordinates and value, can be plotted in ArcGIS

Enter first and last **time step** of movie: 1 to last moviedata files

Moviename: 1 – using frame number, 2 – using timestep

The outputs are saved in OUTPUT_FILES folder.

For a quick look, create movie files in DX and observe it in OpenDX. For a closer and more detailed view create movie files in gmt then plot them in ArcGIS since OPenDX usage is restricted and only allows viewing of files.

Shaking Maps

- Same as creating movie, type

```
make create_movie_AVS_DX
./xcreate_movie_AVS_DX
```

- Choose which **type of files** you want to create as in **steps 3.2**, then instead of entering first step of movie, choose -1 for shaking map

Choose shaking map types

1 – displacement

2 – velocity

3 – acceleration

Choose scale of shaking maps

1 – non linear

2 – non scaling

The outputs are saved in OUTPUT_FILES named DX_shaking_map.dx or gmt_shaking_map.xyz. Beware that each of the shaking maps will be saved with the same name, so make sure to save it with different name before overwriting it.

Synthetic Seismograms

- check the output_list_stations.txt in OUTPUT_FILES folder to see the filtered stations.
- Type:

```
Make convolve_source_timefunction
./xconvolve_source_timefunction
```

NB: Do not be alarmed if an error message appears. For instance, error warning 'input_convolve_code.txt' does not exist but other commands still can run .

- go to UTILS/seis _process
- type `./process_trinet_data.pl` and check out the usage (also can be found in the manual)

Use this command:

`./process_trinet_data_pl –m /home/CMTSOLUTION` (path to CMT SOLUTION file) `–l 1/180 –t 1/40 –I –p –x –bp /home/DATABASES_MPI/BVH.NP.BH?.sem?`

(BVH.NP = name of the stations)

Check the output files *.bp in DATABASES_MPI folder and plot this as a function of time.

Appendix D

Amplification

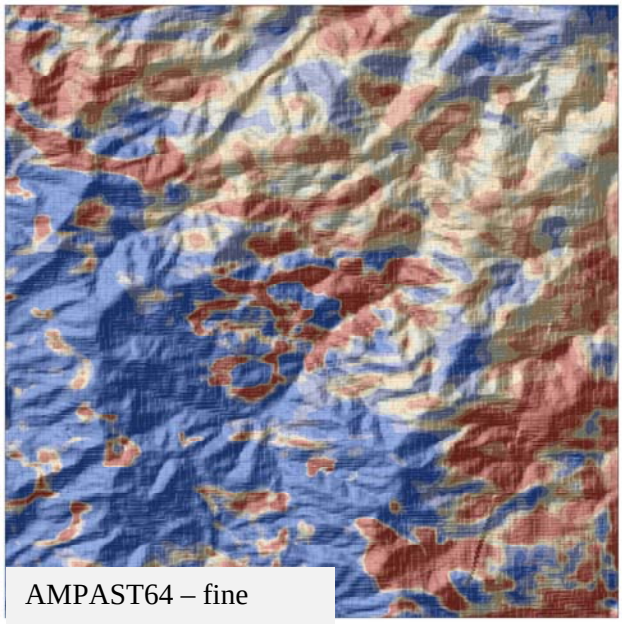

AMPAST64 – fine

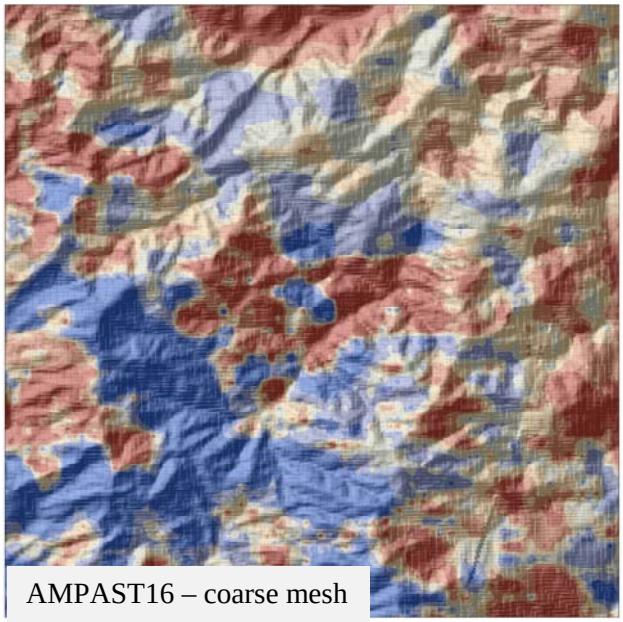

AMPAST16 – coarse mesh

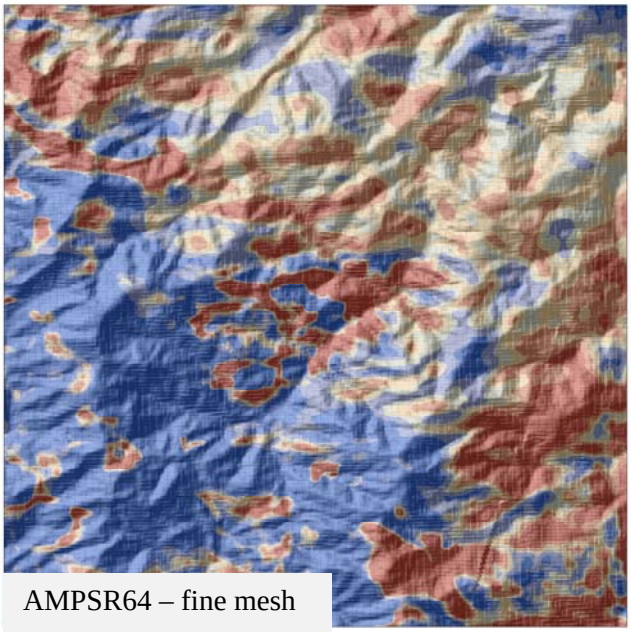

AMPSR64 – fine mesh

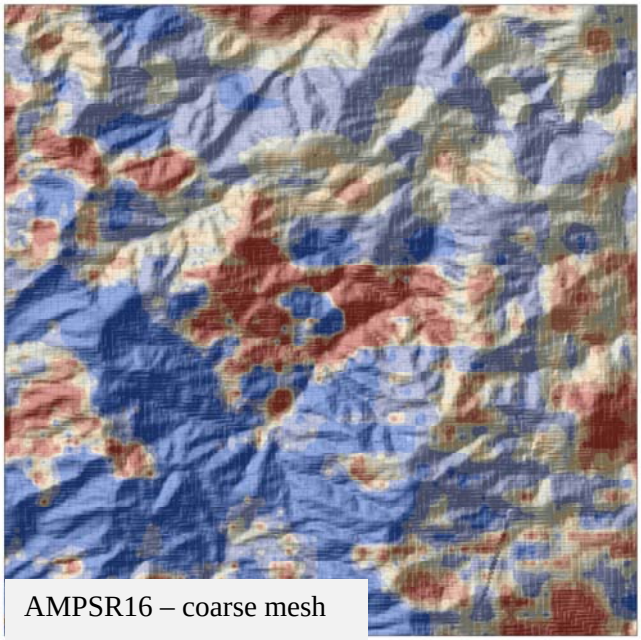

AMPSR16 – coarse mesh